

# Primordial Black Hole Formation in a Dust Bouncing Model

E.J. Barroso,<sup>a,1</sup> L.F. Demétrio,<sup>a</sup> S.D.P. Vitenti,<sup>a</sup> Xuan Ye<sup>b</sup>

<sup>a</sup>Physics Department, Universidade Estadual de Londrina,  
Campus Universitário, CEP 86057-970, Londrina, Brasil,

<sup>b</sup>Department of Astronomy, Key Laboratory for Researches in Galaxies and Cosmology,  
School of Astronomy and Space Sciences, University of Science and Technology of  
China, 96 JinZhai Road, Hefei, Anhui, 230026, China

E-mail: [eduardo.jsbarroso@uel.br](mailto:eduardo.jsbarroso@uel.br), [demetrio.luizfelipe@uel.br](mailto:demetrio.luizfelipe@uel.br), [vitenti@uel.br](mailto:vitenti@uel.br),  
[yyyyy@ustc.edu.cn](mailto:yyyyy@ustc.edu.cn)

**Abstract.** Linear scalar cosmological perturbations have increasing spectra in the contracting phase of bouncing models. We study the conditions for which these perturbations may collapse into primordial black holes and the hypothesis that these objects constitute a fraction of dark matter. We compute the critical density contrast that describes the collapse of matter perturbations in the flat-dust bounce model with a parametric solution, obtained from the Lemaitre-Tolman-Bondi metric that represents the spherical collapse. We discuss the inability of the Newtonian gauge to describe perturbations in contracting models as the perturbative hypothesis does not hold in such cases. We carry the calculations for a different Gauge choice and compute the perturbations' power spectra numerically. Finally, assuming a Gaussian distribution, we compute the primordial black hole abundance with the Press-Schechter formalism and compare it with observational constraints. From our analysis, we conclude that the primordial black hole formation in a dust-dominated contracting phase does not lead to a significant mass fraction of primordial black holes in dark matter today.

---

<sup>1</sup>Corresponding author.

---

## Contents

<b>1</b>	<b>Introduction</b>	<b>1</b>
<b>2</b>	<b>Flat-Dust Quantum Bouncing Background</b>	<b>4</b>
2.1	Additional Hypothesis for Quantization	4
2.2	Wheeler-DeWitt Equation Solutions	5
<b>3</b>	<b>Linear Scalar Perturbations</b>	<b>6</b>
3.1	Gauge Invariant Perturbations	7
3.2	Classical Equations of Motion	9
3.3	Quantization	10
3.4	Adiabatic Vacuum	11
3.5	Numerical Solution	12
3.6	Spectra	13
<b>4</b>	<b>PBH formation during the contracting phase</b>	<b>15</b>
4.1	Formation Criteria	15
4.2	Critical Threshold	17
4.3	$\bar{p} = 0$	20
4.4	$\bar{p} = w\bar{\rho}$	21
4.5	Filtered Variance	23
4.6	Mass Function	25
<b>5</b>	<b>Discussion and Conclusions</b>	<b>27</b>
<b>A</b>	<b>Einstein Equations for Spherical Collapse</b>	<b>29</b>
<b>B</b>	<b>Fluid's Gauge</b>	<b>34</b>

---

## 1 Introduction

Primordial Black Holes (PBHs) are believed to have been formed in the early universe through the collapse of density fluctuations [1–4]. Due to their formation mechanisms, in the inflationary scenario, PBHs can have a wider range of masses from around  $M \sim 5 \times 10^{-29} M_{\odot}$  if formed at Planck time  $t = 10^{-43} s$  and  $M \sim 10^5 M_{\odot}$  if formed at  $t \sim 1 s$ , resulting in several different effects. The study of primordial black holes has yielded insights into various phenomena. They could have contributed to the cosmological density parameter [5, 6]. Their influence in the Cosmic Microwave Background Radiation (CMB) was studied in Ref. [7] and some recent works explored the connection between evaporating PBHs and gravitational waves [8]. There also have been discussions about whether some measurements of gravitational waves could be attributed to primordial black holes [9]. Undoubtedly, the possibility that primordial black holes constitute

a significant fraction of cold dark matter remains a focal point in current research [10], since they are labeled as non-baryonic as their formation takes place before the Big Bang Nucleosynthesis (BBN) [11]. Recent observations of merging binary black holes with unexpected mass ranges by the LIGO/Virgo collaborations indicate that they could have originated from PBHs [12, 13].

Various mechanisms can result in primordial black hole formation (see Ref. [14] for a review). They can originate from the collapse of large isocurvature perturbations of cold dark matter [15], first-order phase transitions [16, 17], critical collapse of matter perturbations [2, 4], and others. Based on the study of critical phenomena and simulations, the formation mass of black holes in this context will heavily depend on the cosmological model and the shape of perturbations [18], which will directly impact the critical threshold  $\delta_c$ . Thus, the density contrast and its critical value must be carefully studied.

In the inflationary scenario [19–22], several studies have analyzed the formation of PBH at the end of inflation [23–26] and in the reheating phase [27, 28] either as a probe for the inflationary model or to analyze the abundance of PBH in dark matter. When confronting the results with combined probes from observational data, it was found that the only acceptable PBH mass range that allows these objects to entirely constitute dark matter is  $10^{-16}M_\odot - 10^{-12}M_\odot$  [29, 30]. Nonetheless, other mass ranges that lead to a smaller fraction of dark matter have intriguing impacts to be considered. For instance, in the mass range  $10^6M_\odot$  to  $10^{10}M_\odot$  where PBHs only represent 0.1% of DM, they could play a role in generating supermassive black holes. In [31] it was also concluded that the possibility of dark matter being constituted by supermassive primordial black holes is viable. However, these results led researchers to study PBH formation in other cosmological models to check the dependency of the mass constraints on the chosen models.

As is well known, the inflationary paradigm alleviates the initial condition problems of the  $\Lambda$ -CDM model but does not completely solve them [20, 32, 33]. For instance, one still needs to assume that a small patch of spacetime was of FLRW type and evolved to become the universe that we now observe, which is modeled via perturbation theory [34]. Alternative models to inflation have been considered, mainly bouncing models (see [35–45] for extensive reviews on bouncing cosmology), which focus on solving the singularity problem by introducing a contracting phase connected to the present expanding phase through a minimal scale factor: a bounce. Classical bouncing models, where exotic matter or modifications of GR are considered, have been analyzed extensively in the literature, mainly in Refs. [33, 45]. In these works, one sees that classical bounces are non-trivial to implement and lead to undesired features such as instabilities and new singularities, which are associated with the violation of the null energy condition.

One may also consider quantum bounces, where the quantization of gravity itself eliminates the primordial singularity. In particular, since quantum bounces do not make use of exotic matter such as the inflaton, there is no need for a reheating phase. This has been achieved in previous works in the framework of Canonical Quantum Gravity [46]. Other relevant proposals are Loop Quantum Cosmology [47, 48] and String Gas

Cosmology [33, 45].

Some recent studies have analyzed the formation of PBH in bouncing models [49–53]. In this context, it is believed that the long duration of the contracting phase plus the diminishing scale factor may lead to an enhancement of PBH formation, resulting in a more significant contribution to the DM density. In [53] it is concluded that a dust-dominated bouncing universe ( $w > 1/3$ ) is robust against the formation of such primordial black holes. In contrast, for a matter-dominated universe ( $w \ll 1$ ), their formation becomes relevant. A similar conclusion is achieved in [52], where they got an enhanced production of PBHs near the bouncing point and utilized the abundance of PBHs in DM to constrain the bouncing model. However, in the same work, it is stated that these constraints are still not well understood due to a lack of precision in numerical computations.

Furthermore, it is still not quite clear how to properly define the critical threshold for PBHs in bouncing cosmology. Different from the inflationary scenario, the contracting phase dynamics lead to growing perturbations that will collapse before becoming super-Hubble. To circumvent this problem, in [53] it is used the argument that the black holes must be larger or equal to the Schwarzschild radius for the given formation mass seeded by the perturbations. However, there is still the need for a more precise definition of the critical contrast in the bouncing scenario. Furthermore, the gauge definition used in previous works may not be the best choice as it leads to large increasing spectra and thus a miscalculation of the energy-density perturbations [54].

In this work, we study the formation of PBH in a quantum dust non-singular bounce and the hypothesis that these structures constitute a fraction of DM today. We consider the single barotropic fluid quantum bouncing model developed in [32, 46, 55] using Canonical Quantum Gravity, which is a conservative approach to the quantization of General Relativity and should hold as an effective theory up to a certain energy scale [32]. We shall focus on the critical collapse of matter perturbations characterized by the density contrast  $\delta$ , such that the perturbations collapse to form black holes when they achieve a given threshold ( $\delta > \delta_c$ ). To perform this analysis, we need to compute the spectra of the perturbations and the critical threshold needed for the distribution of PBHs. We compute the critical threshold in a more detailed approach, using the Tolman-Bondi-Lemaître metric [56, 57] in a similar way as done in [28]. The perturbations' power spectra will be obtained through an algorithm that computes the valid interval for the adiabatic approximation and solves the dynamics of the perturbations. With these results, we will compute the abundance of PBHs and compare our results with other works in bouncing cosmologies.

This paper is divided as follows: Section 2 is devoted to reviewing the quantum bouncing model. In Sec. 3 we define the quantized perturbations around our background and discuss the Gauge problem. In Sec. 4 we describe the general formation criteria for PBHs formed through critical collapse and compute the critical threshold for the the bouncing scenario. In the same section, we compute the PBH mass fraction and abundance in the bouncing model. We discuss and conclude our results in Sec. 5.

## 2 Flat-Dust Quantum Bouncing Background

In this section, we briefly discuss our adopted quantum bouncing background model, for which we follow mostly Refs. [32, 46]. The primary motivation behind considering quantum bounces lies in the necessity to evade the primordial singularity at the end of the contracting phase. Classical General Relativity, as described by the Penrose-Hawking singularity theorems, requires the violation of the null energy condition  $\rho + p \geq 0$  to avoid the singularity, a condition that often leads to instabilities in classical bouncing models.

Our quantum bouncing model is established through the canonical quantization of General Relativity. The flat-dust bounce is thus a contracting universe model with a negative effective energy density that dominates near the bounce, while classical behavior prevails on larger scales. Nonetheless, the quantum contribution is sufficient to avoid the singularity. This approach represents a conservative method in addressing quantum gravity, as it applies the usual Dirac quantization techniques of constrained systems to General Relativity [58].

To apply canonical quantization to GR, we adopt the standard Hamiltonian formalism. The complete Wheeler-De Witt (WdW) equation that will arise from the Dirac quantization poses several challenges that can be solved by assuming some additional hypothesis [32, 55, 59, 60], which we now discuss. However, we should emphasize that the actual bouncing mechanism is irrelevant to our results since the PBHs with relevant scales are formed way before the quantum phase.

### 2.1 Additional Hypothesis for Quantization

The first problem arises because the WdW equation is formulated on superspace, which represents the space of all possible metrics modulo diffeomorphisms and remains poorly understood [59, 61]. Therefore, we shall only perform quantization on a well-behaved sub-space that possesses the required symmetries, a procedure that is known as a mini-superspace quantization. Thus, we quantize only the sub-space of all possible flat FLRW geometries whose line element is given by the form

$$ds^2 = -N^2 dt^2 + \bar{a}^2 \delta_{ij} dx^i dx^j, \quad (2.1)$$

where  $\bar{a}$  is the scale factor,  $N$  is the lapse function and  $\delta_{ij}$  is the Kronecker delta. In this case, all information about the metric is stored in only one degree of freedom, the scale factor  $\bar{a}(t)$  [32].

Another problem is the lack of an explicit time evolution in the Hamiltonian of the theory. This can be seen by attempting to write the conventional Schrödinger equation for the total Hamiltonian and stating the lack of a clear time evolution parameter. This fact is commonly referred to as the Problem of Time in Quantum Gravity [46, 62, 63]. To define a non-trivial propagator, we shall use an intrinsic variable of the system whose classical evolution is monotonic. Subsequently, we require that the classical concept of time emerges from this variable in the classical limit. Let us now apply such considerations and discuss the solutions for this quantization procedure.

## 2.2 Wheeler-DeWitt Equation Solutions

We start by applying the aforementioned considerations to a flat, homogeneous, and isotropic universe containing a single perfect fluid characterized by the equation of state  $p = w\rho$ , with a constant  $w$ . Subsequently, we specialize in the dust case where  $w \approx 0$ . In this framework, the total Hamiltonian takes the form

$$H = N \left( -\frac{\Pi_{\bar{a}}^2}{4\bar{a}} + \frac{\Pi_T}{\bar{a}^{3w}} \right), \quad (2.2)$$

where

$$\Pi_{\bar{a}} \equiv \frac{\partial L}{\partial \dot{\bar{a}}}, \quad (2.3)$$

$$\Pi_T \equiv \frac{\partial L}{\partial \dot{T}}, \quad (2.4)$$

are the canonical momenta associated with the scale factor  $\bar{a}$  and  $T$ , the latter being a variable that describes the fluid's evolution. Also, we denote the cosmic time derivative as  $\frac{\partial q}{\partial t} \equiv \dot{q}$ , which has a dimension of one over length. Remarkably,  $\Pi_T$  appears linearly in the Hamiltonian, and its classical equation of motion is given by  $\dot{T} = N/\bar{a}^{3w}$ , implying  $\dot{T} > 0$  and making  $T$  a monotonic function of classical time. Hence,  $T$  can be used as a time variable, allowing us to write a Schrödinger-like equation by choosing  $N = \bar{a}^{3w} \implies \dot{T} = 1$ . For the details, see Ref. [32].

Canonical quantization is then performed by promoting classical variables to operators satisfying the canonical commutation relations. This process yields the following Wheeler-DeWitt equation for the wavefunction of the universe  $\Psi(\bar{a}, T)$  [46]

$$i \frac{\partial}{\partial T} \Psi(q, T) = \frac{1}{4} \frac{\partial^2}{\partial q^2} \Psi(q, T), \quad (2.5)$$

such that a specific operator factor ordering was chosen to preserve the symmetries of the classical system [59]. Also, we introduced the change of variable

$$q \equiv \frac{2\bar{a}^{\frac{3}{2}(1-w)}}{3(1-w)}. \quad (2.6)$$

Eq. (2.5) resembles a time-reversed free particle Schrödinger equation and, with appropriate boundary conditions, its solutions are wavefunctions of the scale factor  $\bar{a}(T)$ . We turn to the De Broglie-Bohm interpretation [55, 64], such that assuming a Gaussian wavefunction  $\Psi(\bar{a}, T)$ , the Bohmian trajectory solution reads

$$\bar{a}(T) = \bar{a}_B \left[ 1 + \left( \frac{T}{T_B} \right)^2 \right]^{\frac{1}{3} \frac{1}{(1-w)}}, \quad (2.7)$$

where  $\bar{a}_B$  is an integration constant that represents the minimum scale factor value and  $T_B$  is a small arbitrary constant related to the time scale of the bounce. Remarkably,  $\bar{a}(t) \neq 0$  for all  $t$ , which means that this model is non-singular and represents an eternal universe [46]. For a detailed derivation, see [32].

Given that we focus solely on a contracting universe model filled with dust, we set  $w \approx 0$ , simplifying the time variable  $T$  to the conventional cosmic time  $t$ . With the scale factor obtained in Eq. (2.7), we derive its associated Hubble function

$$\bar{H}(t) \equiv \frac{1}{\bar{a}} \frac{d\bar{a}}{dt} = \frac{2}{3} \frac{t}{(t^2 + t_b^2)}, \quad (2.8)$$

and invert (2.7) to obtain

$$t(\bar{a}) = \pm t_b \sqrt{\left(\frac{\bar{a}}{\bar{a}_b}\right)^3 - 1}. \quad (2.9)$$

Eliminating the time  $t$  using (2.9) in (2.8), we find

$$\bar{H}^2 = \frac{4}{9t_b^2} \left( \frac{\bar{a}_b^3}{\bar{a}^3} - \frac{\bar{a}_b^6}{\bar{a}^6} \right), \quad (2.10)$$

which is equivalent to the Friedmann equation

$$\bar{H}^2 = \frac{\kappa c^2}{3} \rho - \bar{H}_0^2 \Omega_{q0} \bar{a}^{-6}, \quad (2.11)$$

where  $\kappa = \frac{8\pi G}{c^4}$  and  $G$  is the gravitational constant. In the above, there is an additional term  $-\bar{H}_0^2 \Omega_{q0} \bar{a}^{-6}$  when compared to the usual Friedmann equation for a classical universe. In our model, the scale factor dynamics mirrors a typical Friedmann equation with a total energy density  $\rho_T = \rho_d + \rho_q$ , where  $\rho_d$  represents the dust energy density and  $\rho_q = -\Omega_q \rho_c \bar{a}^{-6}$  denotes an effective negative energy density accounting for quantum effects that circumvent the primordial singularity [54]. For large-scale factors  $\bar{a} \gg \bar{a}_b$ , Eq. (2.11) and Eq. (2.7) reduce to the classical dust dominated flat FLRW universe. Thus, far from the bounce, we still have a classical behavior, and the quantum corrections only become relevant when  $t \approx t_b$ . With this, we conclude the analysis of our background quantum bouncing model and move to its associated perturbations. In the next sections, we will consider the above quantum bouncing model with  $w \approx 10^{-10}$  and  $x_b = 10^{35}$  and we solve the equations numerically without any approximation.

### 3 Linear Scalar Perturbations

While the universe appears homogeneous and isotropic on large scales, the FLRW metric falls short of providing a precise description of our universe, which presents inhomogeneities that are associated with structure formation, e.g. galaxy clusters, black holes, stars, and others. To characterize the physical universe, we study linear scalar perturbations around our flat contracting background metric described in the previous section. We will then investigate how said perturbations may seed the formation of primordial black holes in the subsequent section. We will from now on characterize background quantities with an overbar and perturbed (physical) quantities without it.

### 3.1 Gauge Invariant Perturbations

We follow mainly the perturbation theory developed in Refs. [34, 43]. Assuming only scalar perturbations, the total metric of the physical space-time is given by

$$ds^2 = -(1 - 2\phi)c^2 dt^2 + \bar{a}\bar{D}_i\mathcal{B}cdtdx^i + \bar{a}^2(1 - 2\psi)\delta_{ij}dx^i dx^j - \bar{D}_i\bar{D}_j\mathcal{E}dx^i dx^j. \quad (3.1)$$

Here,  $\phi$ ,  $\psi$ ,  $\mathcal{B}$  and  $\mathcal{E}$  denote the scalar metric perturbations that we will assume to be much smaller than one [54]. Also,  $\bar{D}_i$  is the spatial covariant derivative in the  $i$ -th direction. Note that our barotropic fluid has no anisotropic pressure.

The metric perturbations are gauge-dependent variables. In cosmology, a gauge can be seen as the freedom in how we connect, or map, the background and physical manifold, and how we choose our coordinate system [54]. Since GR is a covariant theory, this freedom may then be interpreted as a gauge, which may lead to an ambiguous description of perturbations. Depending on the foliation that characterizes the manifold hyper-surfaces and how we define the perturbations around our background, the physical quantities may have different values [34]. Thus, it is recommended that we work with gauge independent variables to carry out our computations and go back to the physical variables at the end when necessary [64].

We define gauge invariant quantities by analyzing their transformations under gauge transformations, such that we can combine different gauge-dependent quantities to form new invariant ones [34]. However, this leads to a freedom on the variable definitions since many combinations of variables may lead to gauge invariant quantities. With this in mind, we define the Bardeen gauge invariant variables [65]

$$\Phi \equiv \phi + \dot{\delta}\sigma, \quad (3.2)$$

$$\Psi \equiv \psi - \frac{\bar{H}\delta\sigma}{c}, \quad (3.3)$$

with

$$\delta\sigma = -(\dot{\mathcal{E}} - \mathcal{B}) + \frac{2\bar{H}\mathcal{E}}{c}. \quad (3.4)$$

It is important to notice that the new variables in Eqs. (3.2)-(3.3), and other gauge invariant variables do not have a physical meaning unless a gauge is chosen. For instance, in the case of the Newtonian gauge,  $\delta\sigma = 0$  and  $\Phi$  represents the Newtonian potential. Hence we must define our gauge invariant quantities such that they represent our desired physical variables when we assume a particular gauge choice.

We are mostly interested in the energy density perturbations that collapse to form PBHs. These perturbations can be examined using the density contrast, defined as

$$\delta \equiv \frac{\delta\rho}{\bar{\rho} + \bar{p}}. \quad (3.5)$$

This variable provides a normalized measurement of the energy density perturbation  $\delta\rho$  around the background matter density field. However, once again we are interested in

its gauge invariant form

$$\tilde{\delta\rho} \equiv \delta\rho - \mathcal{V}\dot{\bar{\rho}}, \quad (3.6)$$

where  $\mathcal{V}$  is the velocity perturbation of the fluid, which has its gauge invariant form

$$\tilde{\mathcal{V}} \equiv \mathcal{V} + \delta\sigma. \quad (3.7)$$

Using the background Einstein equations, we can relate the density contrast to the Bardeen variables and the gauge invariant curvature perturbation  $\zeta$  through the following relations [44, 66]

$$\Psi = \Phi, \quad (3.8)$$

$$-\frac{2\bar{D}^2\Phi}{3\kappa(\bar{\rho} + \bar{p})} = \frac{\tilde{\delta\rho}}{3(\bar{\rho} + \bar{p})}, \quad (3.9)$$

$$\zeta \equiv \Psi + \frac{\bar{H}}{c}\tilde{\mathcal{V}} \quad (3.10)$$

$$\zeta = \frac{3\bar{a}^3}{N^2 z^2 c_s^2} \left[ \frac{\partial}{c\partial t} \left( \frac{c\Phi}{3\bar{H}} \right) + \frac{\Phi}{3} \right], \quad (3.11)$$

$$\bar{D}^2\Phi = -\frac{z^2\bar{H}}{c\bar{a}^3}\dot{\zeta} = -\frac{\bar{H}}{2c\bar{a}^3}\Pi_\zeta. \quad (3.12)$$

For completeness, we also write its relation to the usual Mukhanov-Sasaki variable  $v$ , that is,

$$v \equiv -\zeta z \sqrt{\frac{2}{\kappa c}}. \quad (3.13)$$

We will establish a connection between PBH formation and the density contrast in the next section. For now, it suffices to understand that the excess energy density associated with the perturbations leads to black hole formation, and we can measure such excess through the density contrast. Thus our definition in Eq. (3.6) is extremely important and we will now analyze it.

Note from Eq. (3.6) that if we choose a gauge where  $\mathcal{V} = 0$ ,  $\tilde{\delta\rho}$  becomes the physical density perturbation, which leads to an easier interpretation of this quantity. Also, the choice of  $\mathcal{V} = 0$  will be well suited to connect our perturbation theory with the Lemaitre-Toman-Bondi metric discussed in App. B. Other works have defined the gauge invariant density perturbation as

$$\tilde{\delta\rho}^N \equiv \delta\rho - \delta\sigma\dot{\bar{\rho}}, \quad (3.14)$$

so that this quantity becomes the physical variable in the Newtonian Gauge, where  $\delta\sigma = 0$  and  $\Phi = \phi$ . However, in Ref. [54], it was shown that for bounce models with long contracting phases, regardless of the bounce type, the Bardeen perturbation  $\Phi$  grows

larger than one and invalidates the perturbative series, as  $\phi$  also grows larger than one in the Newtonian Gauge. Additionally, the definition in Eq. (3.14) leads to

$$\zeta = \Phi + \frac{2\bar{D}^2\Phi}{3\kappa(\bar{\rho} + \bar{p})} + \frac{\tilde{\delta\rho}^N}{3(\bar{\rho} + \bar{p})}, \quad (3.15)$$

which implies that  $\tilde{\delta\rho}^N$  grows with  $\Phi$  and thus has larger spectra as well in this gauge. Hence, the Newtonian gauge is not a valid choice for bounce models as it would lead to miss-calculation of the physical quantities whose values would be inflated. We shall avoid this choice in this work and stick with the definition in Eq. (3.6). We now compute the density contrast modes, which require the perturbative equations of motion of the model.

### 3.2 Classical Equations of Motion

The perturbations are described by the Einstein-Hilbert action expanded up to second order, resulting in the Mukhanov-Sasaki Lagrangian

$$L_{MS} = \int d^3\mathbf{x} \frac{1}{\kappa c} \left( \dot{\zeta}^2 z^2 + c_s^2 z^2 \zeta \Delta \zeta \right), \quad (3.16)$$

where  $c_s^2 = \left( \frac{\partial \bar{p}}{\partial \bar{\rho}} \right)_S = w$  is the speed of sound,  $\Delta = \bar{D}^2$  is the spatial Laplacian operator and

$$z^2 = \frac{c^2 \kappa \bar{a}^3 (\bar{\rho} + \bar{p})}{2\bar{H}^2 c_s^2}. \quad (3.17)$$

To compute the density contrast in Eq. (3.9), we will need the curvature modes related to the Mukhanov-Sasaki Lagrangian. The extremization of Eq. (3.16) in Fourier space yields the equation of motion

$$\frac{\ddot{\zeta}_k}{\kappa c} + 2 \frac{\dot{\zeta}_k}{z \kappa c} + \frac{k^2}{\bar{a}^2} \frac{\zeta_k}{\kappa c} = 0, \quad (3.18)$$

where  $k$  is the comoving wave number of the modes. Since obtaining analytical solutions to (3.18) is non-trivial, we will employ a numerical code to compute the modes, which requires the use of dimensionless variables. In dimensionless units, denoted with a subscript  $A$ , we redefine our variables as<sup>1</sup>

$$\zeta_{k_A, A} \equiv \frac{\zeta_k}{\sqrt{8\pi l_p^2 R_H}}, \quad (3.19)$$

$$\Pi_{\zeta_k, A} \equiv \frac{\Pi_{\zeta_k} \sqrt{R_H}}{\sqrt{8\pi l_p^2}}, \quad (3.20)$$

$$k_A \equiv k R_H, \quad (3.21)$$

$$t_A \equiv \frac{ct}{R_H}, \quad (3.22)$$

---

<sup>1</sup>A derivative of a dimensionless variable will also be dimensionless. However, we use the same dot notation.

where  $l_p$  is the Planck length and  $R_H = \frac{c}{H_0}$ . The equation of motion becomes

$$\begin{aligned} \dot{\Pi}_{k_A,A} + \frac{2c_s^2 z^2 k_A^2}{a^2} \zeta_{k_A,A} &= 0 \quad \text{or} \\ \dot{\Pi}_{k_A,A} + 2\omega_{k_a}^2 z^2 \zeta_{k_A,A} &= 0. \end{aligned} \quad (3.23)$$

Here,  $\omega_A^2 \equiv \frac{c_s^2 k_a^2}{a^2}$  is the dimensionless frequency and the dimensionless conjugated momenta are given by

$$\Pi_{k_A,A} = 2z^2 \dot{\zeta}_{k_A,A}. \quad (3.24)$$

Eq. (3.23) can be interpreted as a harmonic oscillator with a time-dependent frequency  $\omega_{k_a}(t_a)$  and mass  $m(t_a) = 2z^2$ . From here on, we are going to use the dimensionless variables with the same notation as described above.

Before solving this system numerically, we need to discuss the quantized version of our modes. This is because we need a prescription to set initial conditions of the perturbative variable  $\zeta$ . We do that by imposing initial vacuum conditions for the quantum fields, and thus, the problem turns into the problem of defining an appropriate vacuum state.

### 3.3 Quantization

In this model, the background is characterized by a quantum contracting phase where an effective quantum fluid dominates near the bounce. Consequently, we seek quantized perturbations for consistency, although both theories can be viewed independently. In particular, the use of quantized perturbations evolving on classical backgrounds has been widely used since the results of Mukhanov and Chibisov [67] and Hawking [68] to derive the power spectrum of primordial perturbations, which are in turn used to describe the formation of structure on our universe.

The use of quantum fields to describe primordial perturbations means that said fields will have statistical properties. We may then partition the universe into local spatial regions and consider each one as a realization of a random process and compare its statistical properties with our theoretical predictions.<sup>2</sup>

We proceed to quantize our fields by promoting them to Hermitian operators that act on a Fock space. In terms of the usual Fourier mode expansion, our quantum operators, denoted with a hat superscript  $\hat{\phantom{x}}$  from now on, are given by

$$\hat{\zeta}(\mathbf{x}, t) = \frac{1}{(2\pi)^{\frac{3}{2}}} \int d^3\mathbf{k} \left( e^{i\mathbf{k}\cdot\mathbf{x}} \zeta_k^*(t) a_k + e^{-i\mathbf{k}\cdot\mathbf{x}} \zeta_k(t) a_k^\dagger \right) \quad (3.25)$$

---

<sup>2</sup>Here, an important remark must be made: in inflationary models, one usually postulates this quantum to classical statistical connection, but the specific mechanism that converts a quantum universe to a classical one is still an open problem [32, 64]. In our model, even if the perturbative level predictions do not depend strongly on the bouncing mechanism if one assumes the De Broglie-Bohm interpretation applied to Canonical Quantum Gravity, this problem is automatically solved [60].

and

$$\hat{\Pi}_\zeta(\mathbf{x}, t) = \frac{1}{(2\pi)^{\frac{3}{2}}} \int d^3\mathbf{k} \left( e^{i\mathbf{k}\cdot\mathbf{x}} \Pi_{\zeta_k}^*(t) a_k + e^{-i\mathbf{k}\cdot\mathbf{x}} \Pi_{\zeta_k}(t) a_k^\dagger \right), \quad (3.26)$$

where  $\mathbf{k}$  is the momentum vector with modulus  $k$  and  $a_k$  and  $a_k^\dagger$  are the annihilation and creation operators respectively. Demanding that the quantum fields satisfy the canonical commutation relations

$$\left[ \hat{\zeta}(\mathbf{x}, t), \hat{\Pi}_\zeta(\mathbf{y}, t) \right] = i\hbar\delta(\mathbf{x} - \mathbf{y}), \quad (3.27)$$

and that the complex modes satisfy

$$\dot{\zeta}_k \zeta_k^* - \zeta_k \dot{\zeta}_k^* = i\hbar, \quad (3.28)$$

$$\dot{\Pi}_k \Pi_k^* - \Pi_k \dot{\Pi}_k^* = i\hbar, \quad (3.29)$$

imply that the creation and annihilation operators  $a_k, a_k^\dagger$  satisfy the usual creation and annihilation algebra

$$[a_{k_1}, a_{k_2}] = [a_{k_1}^\dagger, a_{k_2}^\dagger] = 0 \quad (3.30)$$

and

$$[a_{k_1}, a_{k_2}^\dagger] = \delta(k_1 - k_2). \quad (3.31)$$

Equation (3.28) represents the only constraint for choosing the basis of our problem and it is known as the vacuum normalization. To fully specify our operators and solve Eq. (3.23), we need to set initial conditions that will physically determine the annihilation operator and, consequently, the vacuum state of the theory.

### 3.4 Adiabatic Vacuum

In quantum field theory, due to the non-applicability of the Stone-Von Neumann Theorem, different choices of Hilbert Space that are consistent with the commutation relations in Eq. (3.27) are not unitary equivalent, which means that they lead to different physical predictions [69]. Therefore, one also needs a prescription to construct the associated Hilbert Space of a quantum field theory.

Although in usual Minkowski space-time one may use its symmetries to define the Hilbert space, in curved spacetimes one needs other techniques to construct said space [70]. This problem can be mapped to a choice of operators  $\hat{a}_k$  that annihilate the vacuum state  $|0\rangle$ , which in turn depends on the choice of mode functions  $\zeta_k(t)$  that satisfy the normalization condition in Eq. (3.28) [71]. Since such a condition is preserved by the time evolution, it suffices to choose a set of initial conditions  $\{\zeta_k(t_0), \Pi_k(t_0)\}$  at an initial time  $t_0$  [72].

A widely used prescription to define such a vacuum state is known as the adiabatic vacuum prescription [70, 71]. Its main idea is to set initial conditions by demanding that

the mode functions  $\zeta_k(t)$  coincide with their  $\mathcal{N}$  order adiabatic approximation,  ${}^{(\mathcal{N})}\zeta_k(t)$ . This is implemented if one chooses the initial conditions [70]

$${}^{(\mathcal{N})}\zeta_k(t_0) = \frac{1}{\sqrt{\omega_k(t_0)}} e^{i\alpha_k(t_0)} \quad \text{and} \quad {}^{(\mathcal{N})}\dot{\zeta}_k(t_0) = i\omega_k(t_0)\zeta_k(t_0), \quad (3.32)$$

where  $\omega_k^2 = \frac{c_s^2 k^2}{a^2}$  in our case and  $\alpha_k$  is defined by the relation

$${}^{(\mathcal{N})}\zeta_k(t_0)\dot{\alpha}_k(t_0) = 1. \quad (3.33)$$

Using these initial conditions for the modes, a well-defined vacuum state is obtained, which is in turn used to construct the Fock Space by successive applications of the creation operator  $\hat{a}_k^\dagger$  and their linear combinations [71]. Now that we have defined the appropriate initial conditions for quantization, we may use them to solve the equations of motion in Eq. (3.23) and obtain the mode functions, which we shall do numerically.

### 3.5 Numerical Solution

The equations of motion for the curvature perturbation modes are solved numerically using the Numerical Cosmology library (NumCosmo) [73]. Specifically, the NcmCSQ1D and the NcHIPertAdiab algorithms are employed for this purpose. The equations are split into two parts: one representing a harmonic oscillator with a mass  $m_A$  and the other representing the time evolution of the conjugate momenta  $\Pi_{k_A,A}$  of the modes. Explicitly,

$$\Pi_{k_A,A} = m_A \dot{\zeta}_{k_A,A} \quad (3.34)$$

and

$$\dot{\Pi}_{k_A,A} = -m_A \omega_A^2 \zeta_{k_A,A}, \quad (3.35)$$

The adiabatic vacuum prescription is considered, and the initial conditions for the modes are set according to Eqs. (3.32) up to the fourth order<sup>3</sup>. These initial conditions are used as inputs for the numerical algorithm to compute the Fourier modes of the curvature perturbation modes  $\zeta_{k_A,A}$  and their conjugate momenta  $\Pi_{k_A,A}$ . Also, the numerical code computes the validity of the adiabatic approximation for different intervals of time. To assure the veracity of the code, the algorithms have been validated with unit testing and we compared them with analytical solutions (see [GitHub](#))<sup>4</sup>

---

<sup>3</sup>This is because the adiabatic approximation leads to an asymptotic series, whose precision drops as one goes up to a certain definite order [71]. In particular, the code determines the order of optimal precision.

<sup>4</sup>Also, see the [Jupyter Notebook](#) for an example on the usage of the code.

### 3.6 Spectra

The power spectrum of a theory plays a crucial role in understanding the formation of large-scale structures. The power spectrum also allows one to completely describe the statistics of the problem if the density field is described by Gaussian fluctuations [74]. To compute the power spectrum in our cosmological model, we first calculate the two-point correlation function of the field variable  $\zeta(\mathbf{x}, t_i)$  at an initial time  $t_i$ . This function measures the spatial correlation between fluctuations at different points in space. The correlation function is expressed as an integral over Fourier modes, yielding the desired spatial correlation, and takes the form

$$\begin{aligned} \langle \hat{\zeta}(\mathbf{x}, t_i) \hat{\zeta}(\mathbf{y}, t_i) \rangle &= \frac{1}{(2\pi)^{\frac{2}{3}}} \int d^3\mathbf{k} \left[ |\zeta_k(t_i)|^2 e^{-i\mathbf{k}(\mathbf{x}-\mathbf{y})} \right] \\ &= \int \frac{dk}{k} \left[ P_\zeta(k) \frac{\sin kR}{kR} \right], \end{aligned} \quad (3.36)$$

where  $R = |\mathbf{x} - \mathbf{y}|$  and we performed an integral over solid angles in the last equality. In the above, the power spectrum  $P_\zeta$  is defined as<sup>5</sup>

$$P_\zeta(k) \equiv \frac{k^3 |\zeta_k(t_i)|^2}{2\pi^2}. \quad (3.37)$$

Using Eq. (3.37) and the numerical code described in the last section, we can plot the spectra of the theory in Fig. 1. Once again we have different initial times for the adiabatic limit for distinct modes. We also notice an increasing spectra for all the modes, such that they peak at the bounce time.

As known from the literature, the dust bouncing model has an approximate scale-invariant spectrum, that is

$$P_\zeta(k) \approx Ak^{n_s-1}, \quad (3.38)$$

where  $n_s$  is the spectral index. This is a general feature of single barotropic fluid quantum bouncing models, and the spectral index is related to the equation of state parameter  $w$  by<sup>6</sup>

$$n_s(w) = 1 + \frac{12w}{1 + 3w}, \quad (3.39)$$

which is nearly scale invariant for  $|w| \ll 1$ . However, the usual positive values of  $w$  lead to a blue tilted spectrum  $n_s > 1$ , which differ from CMB observations [75], consistent with the inflationary scenario prediction of a red tilted spectrum with  $n_s \approx 0.96$ . Although the initial power spectrum is not consistent with observations, one must recall that our model is considering a pure dark matter-dominated universe, neglecting the effects of radiation. In particular, it has been suggested [32] that the inclusion of radiation may

<sup>5</sup>Note that the power spectrum is already dimensionless, and thus we can use the same definition with our dimensionless variables as well.

<sup>6</sup>For an explicit semi-analytic derivation, see [46].

lead to a red almost scale-invariant spectrum. Therefore, this model must be understood as a first approximation to a more complete model, which is still under development. Furthermore, since most of the modes that influence our universe have crossed the Hubble horizon during dust domination, this means that this model, even with its simplicity, may still cover relevant information for the future complete model.

This result should not advocate for the prediction failure of the contracting scenario since some works also suggest a blue-tilted spectrum for inflationary models [76, 77]. For instance, in Ref. [78] they discuss the possibility of explaining the recent NANOGrav results with a blue-tilted spectra [79]. Also, the spectra are only dictated by a power law for narrow intervals of momenta, which implies that corrections to Eq. (3.38) must be applied. Nonetheless, we see that the contracting phase produces a nearly scale-invariant spectrum. In the next section, we begin to analyze the primordial black hole formation seeded by the scalar perturbations in our cosmological background.

The resulting plots in Fig. 1 depict the power spectra for a single momentum mode ( $k_a = 0.1$ ) of the curvature perturbation, the Bardeen field variable, the density contrast, and the evolution of the scale factor over time. For visualization purposes, we use the same time parameter as the one in the numerical code, namely,

$$\frac{1}{\cosh(\tau_a)^2} \equiv \left[ 1 + \left( \frac{t}{t_b} \right)^2 \right], \quad (3.40)$$

such that  $\tau_a$  is dimensionless by definition. The plots show an increasing power spectrum for all fields, peaking at the bounce. Note that  $\Phi$  has highly divergent spectra, as discussed previously, which shows the inapplicability of the Newtonian Gauge in this model. Additionally, the scale factor decreases with time until reaching its minimum value at the bounce.

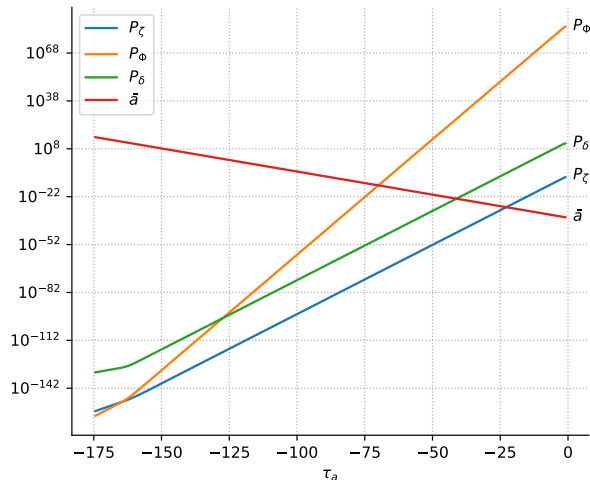


**Figure 1.** Plot of the power spectrum of the curvature perturbation modes  $\zeta_k$ , the Bardeen field variable  $\Phi_k$  and the density contrast  $\delta$  computed with the NumCosmo library for  $w = 10^{-10}$  and  $x_b = 10^{35}$ . The red plot represents the scale factor evolution in time. The time parameter in the x-axis is given by Eq. (3.40).

## 4 PBH formation during the contracting phase

Various mechanisms can result in Primordial black hole formation (see Ref. [14] for a review). In this work, we focus on investigating the formation of primordial black holes through the critical collapse of matter perturbations. This approach has been extensively studied since its popularization by Carr and Hawking [2, 4], and it has found broad applications in the context of inflationary models. We want to extend this approach to the context of a quantum dust-bouncing model and compute the PBH abundance in this scenario. It is important to note that although we perform all the calculations with the gauge invariant variables, we will analyze our results for the physical density perturbation in the fluid’s gauge, as defined in App. B.

### 4.1 Formation Criteria

In our context, critical collapse is the collapse of matter perturbations when they achieve a given threshold. The energy-density perturbation is characterized by the density contrast  $\delta$  defined in Eq. (3.5). We assume that if  $\delta > \delta_c$ , where  $\delta_c$  is the critical threshold, the perturbations will collapse into a black hole. This critical threshold relies both on the cosmological model and the shape of perturbations (see Ref. [18, 80] for a comprehensive analysis of this effect) and therefore must be carefully studied as it will heavily impact the formation of black holes.

The critical collapse model assumes the existence of a region of radius  $r$  with an overdensity  $\delta$ . To compute the probability of the existence of this overdense region, we

will need to compute the variance of our random variable  $\delta$  and instead of working with the original density contrast, we work with its filtered version  $\delta_r$ , which is defined by

$$\delta_r(t) = \int d^3\mathbf{x}' \delta(t, \mathbf{x}') W_r(\mathbf{x} - \mathbf{x}'), \quad (4.1)$$

where  $r$  is a smoothing scale in comoving units related to the mean density by  $M = \frac{4\pi r^3 \bar{\rho}_m}{3}$  and  $W$  is the top-hat filter

$$W_r(\mathbf{x}) = W_r(|\mathbf{x}| = x) = \begin{cases} \frac{1}{4\pi r^3} & \text{if } x \leq r \\ 0 & \text{otherwise} \end{cases}. \quad (4.2)$$

The filter function is used to select a desired scale such that we would only analyze collapsed objects that lie in this interval<sup>7</sup>. In this work, we are using a simple top-hat windowed function for the filter. We usually work on the Fourier space with comoving wave-number  $k$ , such that the filter is given by

$$W_r(k) = \frac{3}{(kr)^2} \left( \frac{\sin(kr)}{kr} - \cos(kr) \right) = \frac{3}{kr} j_1(kr). \quad (4.3)$$

We will see that the filter is necessary to analyze scales where the PBH formation is most likely to happen.

Coming back to  $\delta_r$ , we know from our quantum fields that the density contrast is a random field following a Gaussian distribution with a zero mean. This is also supported by significant research on the statistics of peaks in random Gaussian fields, which can give rise to collapsed objects, as explored in Ref. [81]. Mathematically, the probability of a region with radius  $r$  having an overdensity  $\delta_i$  is given by

$$P(\delta_i) = \frac{1}{\sqrt{2\pi}\sigma_r} \exp\left(-\frac{\delta_i^2}{2\sigma_r^2}\right). \quad (4.4)$$

This Gaussian is completely defined by its variance

$$\sigma_r^2 = \langle \delta_r^2(\mathbf{x}) \rangle \equiv \sigma_r^2 = \frac{1}{2\pi^2} \int_0^\infty \frac{dk}{k} \left[ P_{\bar{\delta}}(k) |W_r(k)|^2 \right], \quad (4.5)$$

where  $P_{\bar{\delta}}(k)$  is given by Eq. (3.37) with the density contrast modes. Unfortunately, for our bounce model, this integral does not converge. Before we perform this calculation, we will analyze the critical threshold for PBH formation, which will lead to scale constraints that will help us solve this problem.

---

<sup>7</sup>Frequently we will usually refer to such scale in terms of the mass  $M$  instead of the comoving radius  $r$  that encloses this mass.

## 4.2 Critical Threshold

In inflationary models, the frozen super-Hubble density perturbations re-enter the Hubble horizon at the end of the potential decay and collapse into a black hole if they have values above the critical threshold [82]. Hence the Hubble horizon is viewed as a characteristic scale for their formation and the threshold ( $\delta_c$ ) is obtained via the Minster-Sharp equations (see Ref. [80]). However, in the bounce scenario, the perturbations constantly evolve in time and there is not only one characteristic scale for the formation, since any perturbation above a critical threshold may collapse as they are not frozen. Thus, we must carefully analyze how to obtain this critical value starting with a local metric for the collapse.

In App. A, we find the solutions for Einstein's equations of a critical collapse represented with a local metric, which led to the LTB set of solutions

$$R(\theta, r) = \frac{r(1 + \delta_{ini})}{\delta_{ini}} \sin^2\left(\frac{\theta}{2}\right), \quad (4.6)$$

$$t(\theta, r) = t_1(r) + \frac{1 + \delta_{ini}}{2\bar{H}_{ini}\delta_{ini}^{\frac{3}{2}}(t_{ini})} (\theta - \pi - \sin\theta). \quad (4.7)$$

In this section, we wish to impose some constraints on those solutions to find the exact point at which the perturbations will form a black hole. Consequently, this will lead to a critical value for the density contrast. First of all, let us analyze the parameter  $\theta$ . From Eq. (A.39),

$$\theta_{ini} = \pm 2 \arcsin\left(\sqrt{\frac{\delta_{ini}}{1 + \delta_{ini}}}\right). \quad (4.8)$$

To choose between the positive or negative value, we use our initial condition in Eq. (A.35) and Eq. (A.34) as a test, such that replacing Eq. (4.8)

$$\left.\frac{\dot{R}}{R}\right|_{ini} = \left.\frac{\frac{\partial R}{\partial \theta}}{R \frac{\partial t}{\partial \theta}}\right|_{ini} = \pm \bar{H}_{ini}. \quad (4.9)$$

From the above, we note that the positive sign in Eq. (4.8) leads to the right definition of our initial conditions. If one chooses the negative sign, and as  $\bar{H}_{ini}$  is negative in the contracting phase, we would end up with an initially expanding patch. This feature can be seen in Fig. 2, where Eqs. (4.6) and (4.7) were solved analytically with Wolfram Mathematica [83]. The blue lines represent the positive choice that leads to the LTB collapse model in a contracting universe, while the orange lines describe an LTB collapse model with an initially expanding patch. On the left side of the figure, for a larger value of  $\delta_{ini}$ , we see that both solutions are similar as the orange plot has an insignificant initial expansion. For a smaller value of  $\delta_{ini}$  on the right, the model in orange first goes on an expansion phase followed by the collapse, while the blue plot is already in a contracting phase and collapses much earlier.

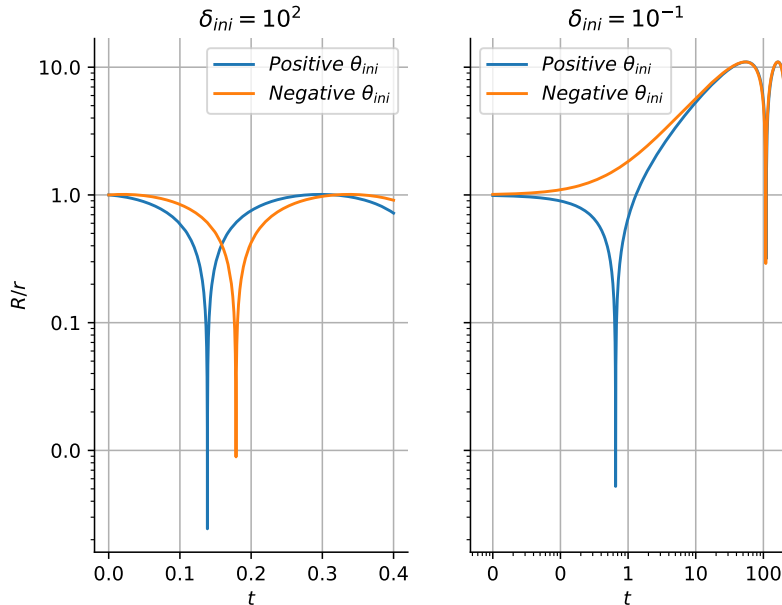


**Figure 2.** Plot of  $R$  vs  $\theta$ . We have chosen  $\bar{H}_{ini} = -1$  for simplification purposes, which implies that  $t$  is in units of  $1/\bar{H}_{ini}$ . On the left side, we see the case for a large initial density contrast while the right side indicates a small initial density contrast. The blue and the orange lines indicate the positive and negative initial conditions for  $\theta_{ini}$  respectively. The blue line represents the right choice and a contracting model while the orange line indicates an expansion model. We chose different values of  $\delta_{ini}$  for both graphs as the difference between both choices becomes more evident for a smaller initial density contrast. The data was computed with Wolfram Mathematica [83] and the graphs were generated in Python.

Let us now analyze the PBH formation. The collapsed object will form a singularity when  $\frac{\partial R}{\partial r} = R' = 0$  [84]. From Eq. (4.6) we see that

$$R' = \frac{(1 + \delta_{ini})}{\delta_{ini}} \sin^2\left(\frac{\theta}{2}\right) = 0 \quad (4.10)$$

if  $\theta = 0$ . Consequently, we want to analyze the necessary time for a black hole to form, which takes place at  $\theta = 0$ . From Eq. (4.7) we have that the final time  $t_f$ , i.e., the time at formation is

$$t_f = t(0, r) = t_1(r) - \frac{\pi(1 + \delta_{ini})}{2\bar{H}_{ini}\delta_{ini}^{\frac{3}{2}}(t_{ini})}. \quad (4.11)$$

We want to compute the formation time  $\Delta t = t_f - t_i$ , such that  $t_i = t(\theta_{ini}, r)$  with

$$\theta_{ini} = 2 \arcsin\left(\sqrt{\frac{\delta_{ini}}{1 + \delta_{ini}}}\right). \quad (4.12)$$

Hence, from Eq. (4.7), we have that

$$\begin{aligned}
\Delta t &= t_f - t_i \\
&= \frac{(1 + \delta_{ini})}{2\bar{H}_{ini}\delta_{ini}^{\frac{3}{2}}} (-\theta_{ini} + \sin \theta_{ini}), \\
&= \frac{(1 + \delta_{ini})}{2\bar{H}_{ini}\delta_{ini}^{\frac{3}{2}}} \left( -2 \arcsin \left( \sqrt{\frac{\delta_{ini}}{1 + \delta_{ini}}} \right) + \sin \left( 2 \arcsin \left( \sqrt{\frac{\delta_{ini}}{1 + \delta_{ini}}} \right) \right) \right). \quad (4.13)
\end{aligned}$$

Assuming that  $\delta_{ini} \ll 1$ , we can expand the above relation such that

$$\Delta t = -\frac{2}{3\bar{H}_{ini}} + \frac{2\delta_{ini}}{15\bar{H}_{ini}} + \mathcal{O}^2(\delta_{ini}). \quad (4.14)$$

We now know how to compute the time interval with the right side of the above equation. We shall now study the left side of Eq. (4.14) as we want to find a constraint on the final formation time  $t_f$ . Supposing that the PBH is formed way before the bounce<sup>8</sup>, we can approximate Eq. (2.8) to

$$\bar{H} = \frac{2}{3t}. \quad (4.15)$$

Plugging this result for  $t_i$  on the left side of Eq. (4.14) leads to

$$t_f = \frac{2\delta_{ini}}{15\bar{H}_{ini}}. \quad (4.16)$$

Let us rewrite the above expression in terms of the redshift function  $x$  defined as

$$x(t) \equiv \frac{\bar{a}_0}{\bar{a}(t)}, \quad (4.17)$$

such that the Hubble function can be written as

$$\bar{H} = -\bar{H}_0 \sqrt{\Omega_w} x^{3/2} \quad (4.18)$$

and thus Eq. (4.16) becomes

$$t_f = -\frac{2\delta_{ini}}{15\bar{H}_0 \sqrt{\Omega_w} x_{ini}^{3/2}}. \quad (4.19)$$

We need to impose a limit on the formation time to find the critical values of delta. For collapsed objects larger than the Hubble radius, their dynamics will be dominated by the FLRW metric and not the LTB approximation. The super-Hubble perturbations will be frozen and thus there is no collapse for these scales. This sets the Hubble length as an upper cut-off, i.e., their formation time must be at most the time for the perturbation

---

<sup>8</sup>We do not make this approximation in the numerical code. This approximation is only used to demonstrate our calculations.

to achieve the Hubble radius, labeled as  $t_H$ . The radius is related to the perturbation's wavelength  $\lambda$  and comoving wavenumber  $k$  by [53]

$$r = \frac{\lambda}{2}, \quad (4.20)$$

$$\lambda = \frac{2\pi}{k}. \quad (4.21)$$

We want to analyze when a perturbation with wavenumber  $k$  has the same size as the Hubble radius, that is,

$$k_H = \frac{1}{x_c} |\bar{H}|. \quad (4.22)$$

From Eq. (4.22) and Eq. (4.18), we have that the redshift function associated with this scale is given by

$$x_H = \frac{k_a^2}{\Omega_w}, \quad (4.23)$$

where  $k_a$  is the comoving dimensionless wave number and the subscript  $H$  indicates the Hubble scale. In terms of time, we can rewrite Eq. (4.23) with Eq. (4.15) and Eq. (4.18) such that

$$t_H = -\frac{2\Omega_w}{3\bar{H}_0 k_a^2}. \quad (4.24)$$

Finally, we must ensure that

$$t_f \leq t_H \text{ or} \\ \delta_{ini} \geq \frac{5\Omega_w^{\frac{3}{2}} x_{ini}^{\frac{3}{2}}}{k_a^3}, \quad (4.25)$$

where we used Eq. (4.19) and Eq. (3.21). From the above, we can see that the critical threshold depends both on the scale and time and it can be set from the saturation of the inequality as

$$\delta_c = \frac{5\Omega_w^{\frac{3}{2}} x_{ini}^{\frac{3}{2}}}{k_a^3}. \quad (4.26)$$

Let us now evaluate two cases: one considering the dark matter as a pressureless fluid and another considering really small but finite pressure.

### 4.3 $\bar{p} = 0$

A pressureless fluid representing dark matter is a good starting point due to its simplicity. In this case, Eq. (4.25) tells us that, for every scale  $k$ , we can always find a sufficient time in the past such that  $x_{ini} \ll 1$ , leading to the collapse of all density perturbations. In

other words, if the universe is old enough, all perturbations will eventually collapse into a black hole until the universe reaches the bounce. If there was no bounce, the universe would completely collapse into black holes and our model would be highly unstable.

It is indeed expected that a fluid with no pressure leads to a total collapse since no forces are opposing the collapse and dust only interacts via gravity. Thus all dark matter that we see today would indeed be contained in primordial black holes. However, this hypothesis was already refuted by some works by constraining the PBH abundance in dark matter based on observational effects (see Refs. [30, 85]). Hence we must consider a dust fluid with a small but nonvanishing equation of state.

#### 4.4 $\bar{p} = w\bar{\rho}$

In the presence of pressure, it is well known that the Jean's length determines the smaller scale sufficient for a black hole to be formed. The pressure forces oppose the collapse and only for scales above this limit a black hole can be formed. Thus, we are interested in the physical radius in Super-Jeans/Sub-Hubble scales, that is,  $r_j < r < r_H$ . The Jeans comoving scale  $k_j$  is given by [53]

$$k_J = \sqrt{\frac{3}{2}} \frac{1}{xc} \frac{|\bar{H}|}{c_s}, \quad (4.27)$$

$$\cdot \quad (4.28)$$

Thus, no structure smaller than the Jeans length can collapse and we have a lower momenta cutoff  $k < k_j$ . Plugging this requirement plus our upper limit in Eq. (4.27) leads to

$$k_H < k \leq k_j \text{ or} \\ \left( \frac{1}{\sqrt{\Omega_w}} \right)^{\frac{3}{2}} > \frac{x^{\frac{2}{3}}}{k^3} \geq \left( \frac{2c_s^2}{3\sqrt{\Omega_w}} \right)^{\frac{3}{2}} \quad (4.29)$$

where we have used Eq. (4.15) and Eq. (4.18). The above relation indicates that for scales/times that do not satisfy the inequality, the perturbation modes do not contribute to PBH formation. Hence we must evaluate the collapse starting between the Jeans-Hubble time and always ending when the perturbations reach the Hubble length. We can see in Fig. 3 the respective Jeans and Hubble time for each different scale. Note that the interval between both times is always constant for all modes, as it depends only on the dark matter equation of state  $w$ . Thus, for smaller  $w$ , the gap between the times increases and the PBH formation is enhanced as there is more time for them to be formed.

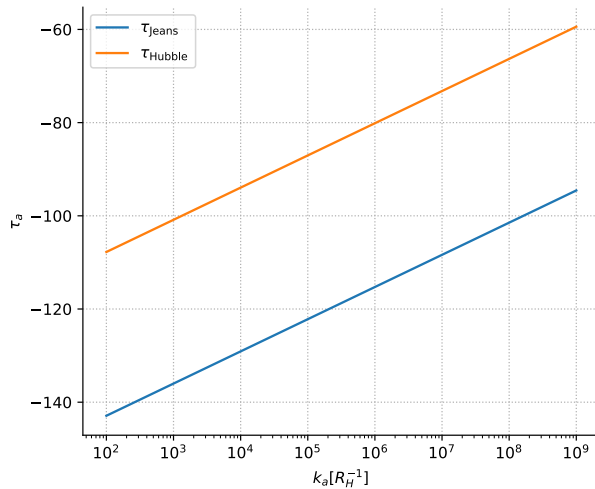


**Figure 3.** Plot of the Jeans and Hubble time computed with the NumCosmo library for  $w = 10^{-10}$  and  $x_b = 10^{35}$ . These times correspond to when the matter density perturbations reach either the Jeans or the Hubble length respectively for each mode  $k$ . The time parameter in the y-axis is given by Eq. (3.40).

Finally, we have the critical threshold in Eq. (4.26) with Eq. (4.29) corresponding to the allowed scales. Hence, not all perturbations will collapse into primordial black holes. Note that for smaller values of  $c_s^2$ , there is more time between the Jeans and the Hubble scale, which allows for more perturbations to collapse. Thus the abundance of PBH in this model is directly related to the equation of state of dark matter, as we will see in the next section.

In this context, let us now analyze Eq. (4.26) for the super-Jeans/Sub-Hubble scales, depicted in Fig. 4. Each plot begins for  $\delta_c$  being computed for  $t_i = t_j$  and goes until  $t_i = t_H$ . The first case corresponds to the collapse starting when the modes just achieved the Jeans length and thus have the maximum amount of time to collapse until reaching the Hubble length. The end of the time interval corresponds to a collapse taking place right before the perturbation reaches the Hubble length, which leads to a maximum value of the critical threshold since there is a minimum amount of time for the collapse of the perturbations. We can see that all plots go from  $\delta_c \approx 10^{-14}$  at Jean crossing time to  $\delta_c \approx 5.0$  at the Hubble scale. However, the closer we get to the Hubble time as the initial time, the worse the approximation  $\delta_c \ll 1$  gets and thus this should be disregarded. If  $t_i = t_H$ , we have that  $\delta_c \sim \infty$ , since there is no time for the collapse to happen. In Fig. 2 we have solved Eq. (4.26) analytically for larger values of  $\delta$ . Nevertheless, such values of density contrast will never be achieved during the contracting phase.

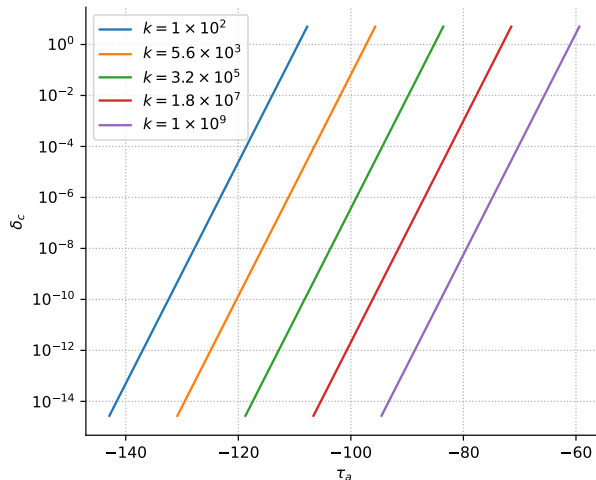


**Figure 4.** Plot of the critical threshold vs time computed with the NumCosmo library for  $w = 10^{-10}$  and  $x_b = 10^{35}$ . Each plot refers to a different scale  $k$ , while points on the same plot represents a different initial time for the collapse. The time interval for each mode starts at the Jeans scale, leading to the smallest threshold values, and ends for initial times when the perturbations reach the Hubble scale, which leads to higher threshold values. The time parameter in the x-axis is given by Eq. (3.40).

#### 4.5 Filtered Variance

Let us now compute the variance which will determine the distribution for PBH. Since sub-Jeans and super-Hubble scales do not contribute to the PBH formation that we are interested in, we want to compute the integral in Eq. (4.5) between  $k_H$  and  $k_j$ . To do so, we first need to evaluate  $P_{\hat{\delta}}(k)$  using Eqs. (3.9)-(3.12) and the field expansions in Eqs. (3.25) and (3.26). Explicitly,

$$\hat{\Psi}(\eta, \mathbf{x}) = \int \frac{d^3\mathbf{k}}{(2\pi)^{\frac{3}{2}}} \frac{\bar{H}}{2c\bar{a}k^2} \left[ \Pi_{\zeta_k} e^{i\mathbf{k}\mathbf{x}} a_k + \Pi_{\zeta_k}^* e^{-i\mathbf{k}\mathbf{x}} a_k^\dagger \right], \quad (4.30)$$

$$\bar{D}^2 \hat{\Psi}(\eta, \mathbf{x}) = - \int \frac{d^3\mathbf{k}}{(2\pi)^{\frac{3}{2}}} \frac{\bar{H}}{2ca^3} \left[ \Pi_{\zeta_k} e^{i\mathbf{k}\mathbf{x}} a_k + \Pi_{\zeta_k}^* e^{-i\mathbf{k}\mathbf{x}} a_k^\dagger \right] \quad (4.31)$$

and

$$\hat{\delta}\rho(\mathbf{x}) = \int_{-\infty}^{\infty} \frac{d^3\mathbf{k}}{(2\pi)^{\frac{3}{2}}} \left\{ \left( \frac{\bar{H}}{c\kappa\bar{a}^3} \right) \Pi_{\zeta_k} e^{i\mathbf{k}\mathbf{x}} a_k + \left( \frac{\bar{H}}{c\kappa a^3} \right) \Pi_{\zeta_k}^* e^{-i\mathbf{k}\mathbf{x}} a_k^\dagger \right\}. \quad (4.32)$$

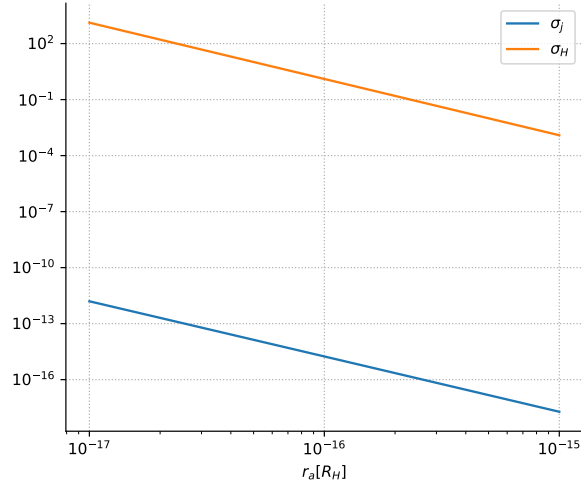


**Figure 5.** Plot of the filtered variance computed with the NumCosmo library for  $w = 10^{-10}$  and  $x_b = 10^{35}$ . Each point corresponds to the variance computed when the perturbations become either the Jeans (blue plot) or the Hubble (orange plot) size for each scale.

Thus, the two-point function and the variance are given by

$$\langle \hat{\delta}(\mathbf{x}) \hat{\delta}(\mathbf{y}) \rangle = \frac{1}{2\pi^2} \int_0^\infty \frac{dk}{k} \left[ P_{\hat{\delta}}(k) \frac{\sin kR}{kR} \right] \quad (4.33)$$

and

$$P_{\hat{\delta}}(k) = |\Pi_{\zeta_k}|^2 \left( \frac{c^2}{9\bar{a}^6 \bar{H}^2 (1+w)^2} \right), \quad (4.34)$$

where we used the flat Friedmann equation

$$\bar{H}^2 = \frac{c^2 \kappa \bar{\rho}}{3}. \quad (4.35)$$

We are now able to compute the variance modes numerically using the above relation together with Eq. (B.5) in the fluid gauge and our numerical code.

The values for the filtered variance computed with Eq. (4.5) from  $k_H$  to  $k_j$  are displayed in Fig. 5. We have plotted the values of  $\sigma_r$  for two different times versus radius. The sub-indexes  $H$  and  $j$  indicate that we are computing the variance at a time when the perturbations are the size of the Jeans length or the Hubble horizon respectively. We can see a linear relation between the filtered variance and the scale radius, such that the former decays with the latter. Larger values of variance indicate a broader Gaussian distribution, which enhances the PBH formation. Thus, from this figure, we see that the formation of PBHs on smaller scales is prioritized rather than on larger scales. We now shall compute the PBH abundance in this model.

#### 4.6 Mass Function

To analyze the abundance of collapsed objects, we use the Press-Schechter (PS) formalism, first proposed in [86]. This ansatz presumes that the objects are formed through a nonlinear collapse and have the property of being universal regarding different cosmological models. Other works have proposed specific mass functions for the primordial black hole production for specific mass ranges, for example [87, 88]. However, in this work, we restrain ourselves to the universal PS formalism to analyze all possible scales. Following this approach, the density of collapsed objects per mass scale is given by the mass function

$$\frac{dn(z, M)}{dM} = -\frac{\bar{\rho}_m(z)}{M} \frac{d\beta(z, M)}{dM}, \quad (4.36)$$

where  $\frac{dn(M, z)}{dM}$  is the mass function,  $z$  is the object's redshift,  $M$  is the object's mass, and  $\beta$  is the fraction of collapsed objects in the mass range of  $M + dM$ .

Assuming that the objects will collapse when  $\delta > \delta_c$ , we can measure the mass fraction inside spheres of radius  $r$  for a time  $t$  that is constituted of collapsed objects as

$$\begin{aligned} \beta(t, r) &\equiv \frac{\rho_{PBH}}{\rho} = \int_{\delta_c}^{\infty} d\delta P(\delta_r) \\ &= \text{erfc} \left( \frac{\delta_c}{\sqrt{2}\sigma_r(t)} \right). \end{aligned} \quad (4.37)$$

However, this function is a probability density of how likely are perturbations to collapse after a time  $t$ . For instance, if we compute it at the time when the perturbations reach the Hubble size,  $\delta_c = \infty$ , this integral will vanish, denoting that there are no more PBHs to be formed after this time. In our context, we are interested in analyzing how many PBHs were formed in the whole contracting phase so we can compute its abundance today. This function shall be given by

$$F(t, r)_{PBH} \equiv \max(\beta(t_i, r)), \text{ for } t_i \leq t. \quad (4.38)$$

The maximum of the beta function indicates for which time there is a higher probability of PBHs to be formed, which will be given by the Jeans time  $t_j$ . Thus  $F(t, r)$  with  $t_i = t_j$  denotes the actual mass fraction of PBHs formed during the entire bouncing

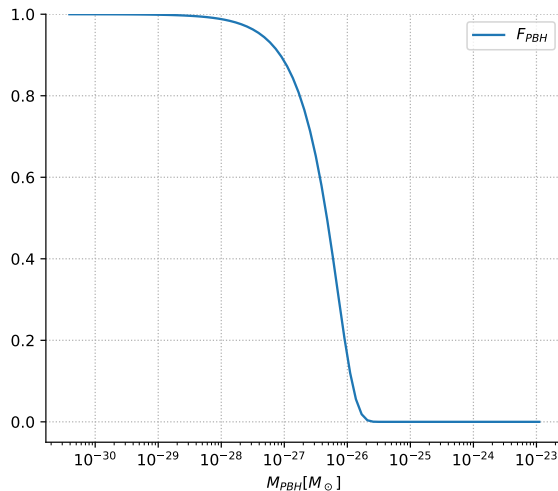


**Figure 6.** Plot of the mass fraction of PBHs forming during bounce versus their formation mass in solar masses for  $w = 10^{-10}$  and  $x_b = 10^{35}$ . The computations were done using the NumCosmo library.

phase. Hence, as an approximation, we will compute the mass fraction for the maximum probability of forming PBHs, i.e., always beginning at  $t_j$ , to find the abundance of PBHs today.

Another crucial quantity is the abundance of collapsed objects in the universe  $\Omega_{PBH}$ , defined in Ref. [89] as the ratio between the density of PBHs and the background universe's density today. This parameter will serve as a guide to compare our theoretical predictions with observational data [30]. Since both the background and the PBHs are formed by dust, both grow with the same power of the scale factor and thus the PBH abundance today will be given by

$$\Omega_{PBH} = F(t, r)\Omega_{DM} = \operatorname{erfc}\left(\frac{\delta_c}{\sqrt{2}\sigma_r(t_j)}\right)\Omega_{DM}. \quad (4.39)$$

In Fig. 6 we can see the values of the density function in Eq. (4.38) for different mass scales. Keep in mind that everything is being computed for the collapse starting at the Jeans time for every scale.

The complementary error function in Eq. (4.37) has higher values when the argument is closer to one, i.e., when the filtered variance and the critical density contrast are in the same scale. We can see in Fig. 6 that this is only true for small mass scales, where the density function is equal to one. However, at these mass scales, every formed PBH black hole would eventually evaporate. From Ref. [30], the evaporation constraint determines that only black holes with masses  $M > 10^{-18}M_\odot$  would have not completely evaporated today. Thus, for larger scales, the density fraction equals zero, and there is

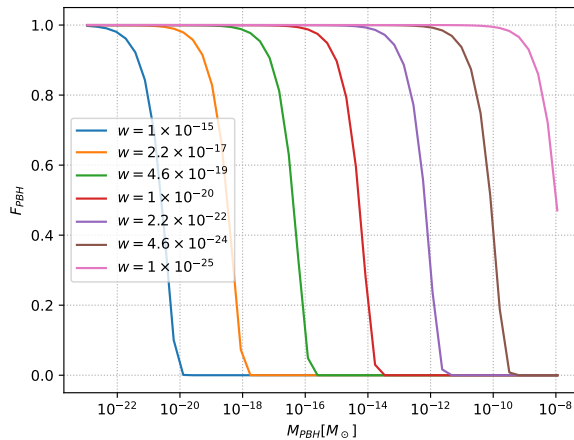


**Figure 7.** Plot of the mass fraction of PBHs forming during bounce versus their formation mass in solar masses for different value of  $w$  and  $x_b = 10^{35}$ . The computations were done using the NumCosmo library.

no relevant PBH formation in this model. Nonetheless, since we are dealing only with dust, which has a small and not completely determined equation of state, let us analyze the same function for different values of  $w$ , depicted in Fig. 7.

For smaller values for the equation of state of cold dark matter, we can see an enhancement in the density function. This case reflects our previous discussion of a pressureless fluid. As we go further into the smaller values, almost every scale will collapse into a black hole and thus the density function equals one.

## 5 Discussion and Conclusions

In this study, we investigated the formation of PBHs in a flat quantum bouncing model containing only dark matter with a small equation of state parameter  $w$ . Despite the spectra from this model exhibiting a slight blue tilt, which deviates from observations of the Cosmic Microwave Background (CMB), this discrepancy should not preclude the model, as the inclusion of radiation is expected to induce a different spectrum that may be compatible with observations [43]. The dark matter-only model serves as an initial attempt to quantify PBH formation during the contracting phase.

Constraints for PBH formation were established, requiring their lengths to fall between the Jeans and Hubble scales. These upper and lower bounds enabled the computation of the critical density contrast, detailed in Sec. 4.2 and App. A. We obtained a time/scale-dependent critical threshold different from the usual constant due to the contracting dynamics. This behavior was expected as there is not only one characteristic scale for the collapse in the bounce model since the perturbations may collapse for any scale between the Jeans and the Hubble scale, which affects the threshold calculation.

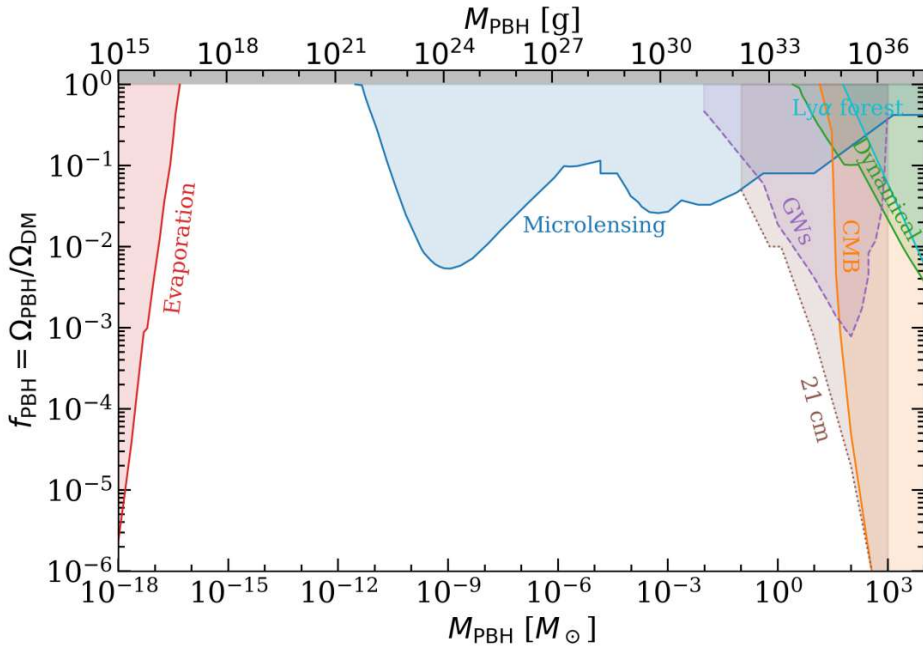


**Figure 8.** Plot of the density function equivalent to the one in Eq. (4.38) versus the formation mass of PBHs. The colored areas are related to Constraints on the PBH fraction constituting dark matter today. Each color corresponds to a different probe considered to constrain PBH abundance. The uncolored area of the graph corresponds to the possible fraction values that agree with all probes. Figure from Ref. [30].

For the case of a pressureless field, perturbations for all scales may collapse and the bounce/contracting phase duration would be the only constraint for PBH formation.

For a small but non-zero pressure, we computed the mass fraction of primordial black holes in the universe today, given by Eq. (4.38). In Fig. 6, for a fixed value of  $w$ , we can see an enhancement of the density function for smaller mass scales of PBHs. However, for  $w = 10^{-10}$ , the formed primordial black holes would have such small masses at smaller scales that they would have evaporated completely today. Figure 8 was generated in Ref. [30] by imposing observational constraints on the mass fraction of PBHs. They considered a range of effects such as black hole evaporation, microlensing, gravitational wave measurements, and others. The white regions of the graph correspond to accepted values of the mass fraction and the colored represent physical observational effects that exclude the possibility of PBHs constituting DM in that mass range. We can see that PBHs under the mass range  $M < 10^{-18} M_\odot$  are disregarded due to evaporation, which implies that the formed PBHs depicted in Fig. 6 would have completely evaporated today.

Still on Fig. 6, for larger scales, there is no significant formation as the time interval

for the collapse is not sufficient nor is the variance large enough. Also, the variance decreases with scale, as seen in Fig. 5, while the critical threshold remains constant as it is always computed for the Jeans time at the given scale. Hence the complementary error function decreases since the argument grows and the PBH fraction becomes insignificant.

We have seen in Eq. (4.29) that the time interval for which the perturbations become super-Jeans/sub-Hubble is proportional to  $c_s^3 = w^{\frac{3}{2}}$ . Thus smaller values for the equation of state allow for more time for the perturbations to collapse and therefore enhance the primordial black hole formation. In Fig. 7, we see that only models featuring sufficiently small values for the equation of state of dark matter ( $w < 10^{-17}$ ) may lead to a non-vanishing mass fraction of primordial black hole at relevant scales ( $M > 10^{-18} M_\odot$ ). If we go even further on small values of  $w$ , more scales start to collapse as we have  $F \sim 1$  for all scales as we approach the pressureless fluid scenario.

Another approach for dark matter would be to consider a non-zero temperature. In Ref [90] dark matter is treated as a non-relativistic gas and, even for cases where  $w \ll 1$ , the non-vanishing temperature would erase structure formation for scales smaller than the corresponding free-streaming length, which once again would contribute to decrease PBH formation in this model. If we treat DM as a relativistic gas, its temperature grows with  $\bar{a}^{-2}$  [66]. Thus, its temperature and pressure would diverge close to the bounce and prevent the collapse and PBH formation. We conclude that the formation of PBHs in the flat-dust bounce in observable scales is improbable as the analysis is robust against the formation on larger scales, leading to an insignificant fraction of PBHs as DM today.

The next phase of this research would be to apply the same methodology to a universe populated with radiation and dark matter, which more closely resembles the physical universe and the interaction between both fluids may affect PBH production. If such a model proves reasonable, it would also be interesting to improve the computation of the LTB model in App. A for larger values of the equation of state. Despite the Jeans scale being a good approximation, the introduction of a non-pressureless fluid would also require the study of the pressure impact in our characteristic scales. Furthermore, in a radiation-dominated quantum bouncing model, one expects a greater blue tilt on the spectral index, which may affect the density contrast modes for smaller scales. Said effect could lead to a larger formation of PBHs. This analysis is left for future work.

## A Einstein Equations for Spherical Collapse

In this Appendix, we are interested in solving the Einstein equations for a metric representing the spherical collapse. We intend to use these solutions to compute the critical threshold in Sec. 4.2. We adapted the calculations initially done in Ref. [91] and corrected by Ref. [28]. In these references, a scalar field is used as the source for the energy-momentum tensor. We shall now perform the same calculations for a pressureless barotropic fluid.

An inhomogeneous but spherically symmetric space can be represented by the met-

ric<sup>9</sup>

$$ds^2 = -c^2 dt^2 + e^{-2\Lambda(t,r)} dr^2 + R^2(t,r) (d\theta^2 + \sin^2 \theta d\varphi^2), \quad (\text{A.1})$$

where  $\Lambda(r, t)$  and  $R(t, r)$  are functions of the local coordinates to be defined and we are considering spherical coordinates. Since none of these functions do not depend on the angular variables, this metric may represent any type of spherical collapse. To find the local functions that describe our problem, we need to solve Einstein's equations for an energy-momentum tensor that corresponds to our symmetries. We shall represent  $\partial_r \equiv '$ .

Following [28], the Einstein's tensor components are

$$G_{tt} = \frac{1}{R^2} \left[ 1 + \dot{R}^2 - 2\dot{\Lambda}\dot{R}R - Re^{2\Lambda} \left( 2\Lambda'R' + 2R'' + \frac{R'^2}{R} \right) \right] \quad (\text{A.2})$$

$$G_{tr} = -\frac{2}{R} \left( \dot{R}' + \dot{\Lambda}R' \right) \quad (\text{A.3})$$

$$G_{rr} = \frac{1}{R^2} \left[ R'^2 - e^{-2\Lambda} \left( \dot{R}^2 + 2R\ddot{R} + 1 \right) \right] \quad (\text{A.4})$$

$$G_{\theta\theta} = \sin^{-2} \theta G_{\varphi\varphi} = R \left( \dot{R}\dot{\Lambda} + \Lambda'R'e^{2\Lambda} + R''e^{2\Lambda} - \ddot{R} + \ddot{\Lambda}R - R\dot{\Lambda}^2 \right). \quad (\text{A.5})$$

We want to consider an isotropic and inhomogeneous barotropic fluid. Thus our energy-momentum tensor will have the form of a perfect fluid

$$T_{\mu\nu} = (\rho(r, t) + p(r, t))u_\mu u_\nu + p(r, t)g_{\mu\nu} \quad (\text{A.6})$$

where  $u_\mu u^\mu = -1$  is the velocity vector of the fluid, which we assume to be orthogonal to the spatial hypersurfaces. It is worth mentioning that in Eq. (A.6), both the pressure and the energy density depend on the spatial radius since we want to consider a physical metric modeled as a perturbation around the background quantities. Also, the equation of state parameter of the fluid is

$$w = \frac{p}{\rho} \quad (\text{A.7})$$

and we are considering  $w \ll 1$  for cold dark matter. In this context, the energy-momentum tensor components are

$$T_{uu} = \rho(t, r) \quad (\text{A.8})$$

$$T^r_r = T^\theta_\theta = T^\varphi_\varphi = p(t, r) \quad (\text{A.9})$$

$$T^r_u = 0, \quad (\text{A.10})$$

$$T_{ru} = 0, \quad (\text{A.11})$$

where the indexes  $u$  and  $r$  indicate both the fluid's velocity direction and the radial direction respectively. Let us now move to the Einstein's equations (EE).

---

<sup>9</sup>This metric can also be written with a lapse function that shifts the time component. However, one can always redefine the coordinate to incorporate this quantity.

We can redefine our variables as

$$k(t, r) = 1 - R'^2 e^{2\Lambda}, \quad m(t, r) = \frac{R}{2} (\dot{R}^2 + k), \quad (\text{A.12})$$

such that the EE will be given by

$$k' = \frac{8\pi G}{c^2} R R' (T_{uu} + T^r_r) + 2R' (\ddot{R} + \dot{\Lambda} \dot{R}), \quad (\text{A.13})$$

$$\dot{k} = \frac{8\pi G}{c^2} R R' T^r_u, \quad (\text{A.14})$$

$$m' = \frac{4\pi G}{c^2} R^2 R' T_{uu} - \frac{4\pi G}{c^4} R^2 \dot{R} T_{ru}, \quad (\text{A.15})$$

$$\dot{m} = \frac{4\pi G}{c^2} R^2 R' T^r_u - \frac{4\pi G}{c^2} \dot{R} R^2 T^r_r. \quad (\text{A.16})$$

Additionally, the energy conservation of  $T^{\mu\nu}$  gives the constraint

$$\begin{aligned} \nabla_\mu T^{\mu\nu} &= 0, \text{ or} \\ \nabla_\mu (\rho u^\mu u^\nu + p \gamma^{\mu\nu}) &= (\dot{\rho} + \Theta(\rho + p)) u^\nu = 0. \end{aligned} \quad (\text{A.17})$$

Thus, our system is given by

$$ds^2 = -c^2 dt^2 + \frac{(R')^2}{1-k} dr^2 + R^2(t, r) (d\theta^2 + \sin^2 \theta d\varphi^2) \quad (\text{A.18})$$

with

$$k' = \frac{8\pi G}{c^2} R R' (\rho + p) + 2R' (\ddot{R} + \dot{\Lambda} \dot{R}), \quad (\text{A.19})$$

$$\dot{k} = 0, \quad (\text{A.20})$$

$$m' = \frac{4\pi G}{c^2} R^2 R' \rho \quad (\text{A.21})$$

$$\dot{m} = -\frac{4\pi G}{c^2} \dot{R} R^2 p = -(4\pi G) \dot{R} R^2 \omega \rho = 0. \quad (\text{A.22})$$

plus Eqs. (A.7) and (A.17). One can replace Eqs. (A.22) and (A.20) into (A.19) using the definitions in (A.12) yielding the final equations

$$m' = \frac{4\pi G}{c^2} R^2 R' \rho \quad (\text{A.23})$$

$$(\dot{R})^2 = \frac{2m}{R} - k. \quad (\text{A.24})$$

We can recognize in Eqs. (A.23) and (A.24) the Lemaitre-Tolman-Bondi (LTB) class of solutions [57]. One may check that the metric in Eq. (A.18) describes the Schwarzschild metric if  $m$  is constant, the Einstein-de Sitter universe if  $R = a(t)r$  and  $k = 0$  and the closed Friedmann universe if  $R = a(t)r$  and  $k = r^2$ . We want to find analytical solutions for the system without considering a specific type of these local functions. Luckily, the

LTB class of solutions is one of the few cases where there is an analytical parametric solution to Einstein's field equations, given by

$$R(\theta, r) = \frac{2m}{k} \sin^2\left(\frac{\theta}{2}\right) \quad (\text{A.25})$$

$$t(\theta, r) = t_1(r) + \frac{m}{k^{\frac{3}{2}}} (\theta - \pi - \sin\theta). \quad (\text{A.26})$$

In the above,  $\theta$  is a parameter in the range  $[-2\pi, 0]$  and  $t_1$  is an integration constant<sup>10</sup>. We still have to find  $m$  and  $k$ , which will require initial conditions. Let us first analyze  $m$ .

From the right side of Eq. (A.23), we see that  $m$  is related to the mass density of a spherical volume. To analyze this quantity, we start by rewriting the energy density from the spherical collapse metric as

$$\rho(t, r) = \bar{\rho}(t)(1 + \delta(t, r)), \quad (\text{A.27})$$

such that  $\delta$  is the density contrast  $\delta = \frac{\rho(t, r) - \bar{\rho}(t)}{\bar{\rho}(t)}$  and  $\bar{\rho}$  the background energy density. We consider that there is a small overdensity in our spherical system when compared to the background density. We want to study a top-hat spherical collapse so that outside the over-dense spherical shell characterized by a critical radius  $r_c$ , the energy density is approximately the background density, i.e.,  $(r > r_c) \rightarrow \rho \approx \bar{\rho}$ . We can add this information to the density contrast by making the redefinition

$$\delta(t, r) \rightarrow \delta(t, r)\Theta(r - r_c) \quad (\text{A.28})$$

where  $\Theta$  is the Heaviside function. In this context, Eq. (A.23) becomes

$$m(r) = \int_0^r dr_1 \frac{4\pi GR^2 R'}{c^2} (\bar{\rho} + \delta\Theta(r - r_c)). \quad (\text{A.29})$$

We still have freedom in our metric to define the local function  $R$ , which can be fixed with initial conditions. The simplest choice would be that at initial collapse time  $t_{ini}$ ,  $R(t_{ini}, r) = r$ , which implies that the 3-dimensional spherical shell is initially at rest<sup>11</sup>. This leads to

$$m(r) = \frac{4\pi r^3 G \bar{\rho}(t_{ini})}{3c^2} \left( 1 + \frac{3}{r^3} \int_0^r dr_1 (r_1)^2 \delta(t_{ini}, r_1) \Theta(r - r_c) \right). \quad (\text{A.30})$$

The integral represents the expected value of the density contrast inside a spherical region with radius  $r$  and  $m$  gives the total mass inside this region. To evaluate it, we need to assume that at the initial time, our spherical metric possesses the same symmetries as

<sup>10</sup>Our definition of the parameter  $\theta$  differs from Ref. [28] by  $-\pi$  for simplification purposes.

<sup>11</sup>Note that any other initial condition is valid and sufficient to completely define  $m$ .

the background and thus it is homogeneous. This means that the density contrast has a uniform distribution and does not depend on position at  $t_{ini}$ <sup>12</sup>. Consequently,

$$\delta(t_{ini}, r) = \delta(t_{ini}) \equiv \delta_{ini}. \quad (\text{A.31})$$

We are representing any variable  $V$  at initial time  $t_{ini}$  as  $V(t_{ini}) \equiv V_{ini}$  to simplify the notation. Plugging Eq. (A.31) in (A.30) leads to

$$m(r) = \begin{cases} M \left( \frac{r^3}{r_c^3} \right) & r \leq r_c \\ M + \frac{M}{1+\delta_{ini}} \left( \frac{r^3}{r_c^3} - 1 \right) & r > r_c \end{cases}, \quad (\text{A.32})$$

such that we rewrote the terms as a function of

$$M = m(r_c) = \frac{4\pi G \bar{\rho}_{ini} r_c^3}{3c^2} (1 + \delta_{ini}). \quad (\text{A.33})$$

We may now compute  $k$  using the second relation in Eq. (A.12), which requires us to evaluate  $\dot{R}(t, r)$ . To do so, we define the inhomogenous Hubble function

$$H \equiv \frac{\dot{R}(t, r)}{R(t, r)}. \quad (\text{A.34})$$

Since we have the vanishing relations in Eqs. (A.22) and (A.20),  $R$  is the only local degree of freedom that evolves in time and provides the dynamics of the universe according to Eq. (A.25). Hence it is natural that we use this quantity to define the Hubble function. Assuming that the local metric is homogeneous at  $t_{ini}$ ,

$$H^2(t_{ini}, r) = \bar{H}^2(t_{ini}) = \frac{\kappa \bar{\rho} c^2}{3} = \frac{2M}{1 + \delta_{ini}} \frac{1}{r_c^3}. \quad (\text{A.35})$$

Thus, we can use this relation to compute  $k$  for  $t = t_{ini}$  since this variable does not evolve in time, which leads to

$$k(r) = \frac{2m}{r} - r^2 H_{ini}^2 = \begin{cases} 2M \frac{\delta_{ini}}{1+\delta_{ini}} \frac{r^2}{r_c^3} & r \leq r_c \\ 2M \frac{\delta_{ini}}{1+\delta_{ini}} \frac{1}{r} & r > r_c \end{cases}. \quad (\text{A.36})$$

Now that we have properly computed our local quantities, we can rewrite our solutions in Eq. (A.25) and (A.26) for  $r \leq r_c$  as

$$R(\theta, r) = \frac{r(1 + \delta_{ini})}{\delta_{ini}} \sin^2 \left( \frac{\theta}{2} \right), \quad (\text{A.37})$$

$$\Delta t(\theta, r) = \frac{1 + \delta_{ini}}{2H_{ini} \delta_{ini}^{\frac{3}{2}}(t_{ini})} (\theta - \pi - \sin \theta), \quad (\text{A.38})$$

such that  $\Delta t = t_i - t_j$  for arbitrary times and  $\theta_{ini}$  is obtained from Eq. (A.25) at  $t_{ini}$ , i.e.,

$$\sin^2 \left( \frac{\theta_{ini}}{2} \right) = \frac{\delta_{ini}}{1 + \delta_{ini}}. \quad (\text{A.39})$$

We are now able to use these solutions to compute the critical value for the density contrast.

<sup>12</sup>This is only true at  $t_{ini}$ . At later times, the perturbation evolves and depends on the radial position.

## B Fluid's Gauge

In the last appendix, we computed the solution for the Einstein equations for an inhomogeneous dust-perfect fluid with a spherically symmetric local metric. To use this solution and compare it with our perturbations defined in Sec. 3, we must ensure that measurements in the local metric are in the same Gauge as our perturbations. Since we projected the energy-momentum tensor in the direction of the velocity of the fluid in Eq. (A.8), we consider the Gauge where the fluid is at rest and we shall now see how to define our perturbation theory in this Gauge choice.

Essentially, following [92], we want to make sure that the local tensor in (A.6) can be seen as the perturbed energy-momentum tensor  $\delta T_{\mu\nu}$ . Explicitly, we want

$$T_{\mu\nu} \propto \delta T_{\mu\nu} = (\delta\rho - 2\phi)n_\mu n_\nu + 2(\rho + p)n_{(\mu}\bar{D}_{\nu)}\mathcal{V} + (\delta p\psi) h_{\mu\nu} + 2p(n_{(\mu}\bar{D}_{\nu)}\mathcal{B} + \bar{D}_\mu\bar{D}_\nu\mathcal{E}), \quad (\text{B.1})$$

where we consider no anisotropic pressure. Thus, the fluid's Gauge is obtained by setting

$$\mathcal{V} = \mathcal{E} = 0 \quad \text{and} \quad (\text{B.2})$$

$$\mathcal{B}|_{t_1} = 0. \quad (\text{B.3})$$

With these Gauge choices,

$$\delta T_{\mu\nu} = (\delta\rho - 2\phi)n_\mu n_\nu + (\delta p\psi) h_{\mu\nu} + 2p(\bar{D}_\mu\bar{D}_\nu\mathcal{E}). \quad (\text{B.4})$$

The first choice for  $\mathcal{V}$  in Eq. (B.2) assures that the perturbed fluid is at rest with the background universe. The other two conditions guarantee that, at least for an initial time  $t_1$ , there are no off-diagonal terms and we have an isotropic perturbed fluid. For different times, it is not possible to set a Gauge such that  $\mathcal{E} = 0$  for  $t \neq t_1$  [54]. Nonetheless, we can argue that this term is proportional to the pressure of the fluid which has an almost vanishing value for cold dark matter and thus can be discarded. Also, since our main goal is to make proper measurements of the density contrast that depends on Eq. (3.6), this term is not relevant to our computations. Finally, in the fluid's Gauge, the gauge-invariant density contrast may be interpreted as its physical equivalent, that is,

$$\tilde{\delta\rho} = \delta\rho + \mathcal{V}\dot{\bar{\rho}} = \delta\rho \quad (\text{B.5})$$

where we used Eq. (3.6).

## Acknowledgments

SDPV acknowledges the support of CNPq of Brazil under grant PQ-II 316734/2021-7. EJB acknowledges the support of CAPES under the grant DS 88887.510837/2020-00. LFD acknowledges the support of CAPES under the grant DS 88887.902808/2023-00. We thank Nelson Pinto-Neto and Sheng-Feng Yan for their valuable discussions.

## References

- [1] Ya. B. Zel'dovich and I. D. Novikov. The Hypothesis of Cores Retarded during Expansion and the Hot Cosmological Model. *Soviet Astronomy*, 10:602, February 1967.
- [2] Stephen Hawking. Gravitationally collapsed objects of very low mass. *Monthly Notices of the Royal Astronomical Society*, 152(1):75–78, 1971.
- [3] Stephen W Hawking. Black hole explosions? *Nature*, 248(5443):30–31, 1974.
- [4] Bernard J Carr and Stephen W Hawking. Black holes in the early universe. *Monthly Notices of the Royal Astronomical Society*, 168(2):399–415, 1974.
- [5] B. J. Carr. The primordial black hole mass spectrum. 201:1–19, October 1975.
- [6] Il Hee Kim and Chul H Lee. Constraints on the spectral index from primordial black holes. *Physical Review D*, 54(10):6001, 1996.
- [7] Massimo Ricotti, Jeremiah P Ostriker, and Katherine J Mack. Effect of primordial black holes on the cosmic microwave background and cosmological parameter estimates. *The Astrophysical Journal*, 680(2):829, 2008.
- [8] Guillem Domènech, Volodymyr Takhistov, and Misao Sasaki. Exploring evaporating primordial black holes with gravitational waves. *Physics Letters B*, 823:136722, dec 2021.
- [9] Sai Wang and Zhi-Chao Zhao. GW200105 and GW200115 are compatible with a scenario of primordial black hole binary coalescences. *The European Physical Journal C*, 82(1), jan 2022.
- [10] G. F. Chapline. Cosmological effects of primordial black holes. *Nature*, 253(5489):251–252, January 1975.
- [11] Richard H Cyburt, Brian D Fields, and Keith A Olive. Primordial nucleosynthesis in light of wmap. *Physics Letters B*, 567(3-4):227–234, 2003.
- [12] Benjamin P Abbott, R Abbott, TD Abbott, MR Abernathy, F Acernese, K Ackley, C Adams, T Adams, P Addesso, RX Adhikari, et al. Binary black hole mergers in the first advanced ligo observing run. *Physical Review X*, 6(4):041015, 2016.
- [13] BP Abbott, R Abbott, TD Abbott, S Abraham, Fausto Acernese, K Ackley, C Adams, Rana X Adhikari, VB Adya, C Affeldt, et al. Binary black hole population properties inferred from the first and second observing runs of advanced ligo and advanced virgo. *The Astrophysical Journal Letters*, 882(2):L24, 2019.
- [14] Albert Escrivà, Florian Kuhnel, and Yuichiro Tada. Primordial black holes, 2023.
- [15] Samuel Passaglia and Misao Sasaki. Primordial black holes from CDM isocurvature perturbations. *Physical Review D*, 105(10), may 2022.
- [16] M. Yu. Khlopov, R. V. Konoplich, S. G. Rubin, and A. S. Sakharov. Formation of black holes in first order phase transitions, 1998.
- [17] Jing Liu, Ligong Bian, Rong-Gen Cai, Zong-Kuan Guo, and Shao-Jiang Wang. Primordial black hole production during first-order phase transitions. *Physical Review D*, 105(2), jan 2022.
- [18] Jens C Niemeyer and Karsten Jedamzik. Near-critical gravitational collapse and the initial mass function of primordial black holes. *Physical Review Letters*, 80(25):5481, 1998.

- [19] A. A. Starobinskii. Spectrum of relict gravitational radiation and the early state of the universe. *ZhETF Pis ma Redaktsiu*, 30:719–723, 1979.
- [20] Alan H. Guth. The inflationary universe: A possible solution to the horizon and flatness problems. *Phys. Rev. D*, 23:347–356, 1981.
- [21] James M Bardeen, Paul J Steinhardt, and Michael S Turner. Spontaneous creation of almost scale-free density perturbations in an inflationary universe. *Physical Review D*, 28(4):679, 1983.
- [22] Andrei D Linde. A new inflationary universe scenario: a possible solution of the horizon, flatness, homogeneity, isotropy and primordial monopole problems. *Physics Letters B*, 108(6):389–393, 1982.
- [23] James S Bullock and Joel R Primack. Non-gaussian fluctuations and primordial black holes from inflation. *Physical Review D*, 55(12):7423, 1997.
- [24] Jun’ichi Yokoyama. Chaotic new inflation and formation of primordial black holes. *Physical Review D*, 58(8):083510, 1998.
- [25] Amandeep S Josan and Anne M Green. Constraints from primordial black hole formation at the end of inflation. *Physical Review D*, 82(4):047303, 2010.
- [26] Guillermo Ballesteros and Marco Taoso. Primordial black hole dark matter from single field inflation. *Physical Review D*, 97(2):023501, 2018.
- [27] Bernard Carr, Konstantinos Dimopoulos, Charlotte Owen, and Tommi Tenkanen. Primordial black hole formation during slow reheating after inflation. *Physical Review D*, 97(12):123535, 2018.
- [28] Jérôme Martin, Theodoros Papanikolaou, and Vincent Vennin. Primordial black holes from the preheating instability in single-field inflation. *Journal of Cosmology and Astroparticle Physics*, 2020(01):024, 2020.
- [29] Bernard Carr and Florian Kühnel. Primordial black holes as dark matter candidates. *SciPost Physics Lecture Notes*, page 048, 2022.
- [30] Pablo Villanueva-Domingo, Olga Mena, and Sergio Palomares-Ruiz. A brief review on primordial black holes as dark matter. *Frontiers in Astronomy and Space Sciences*, 8:681084, 2021.
- [31] Juan García-Bellido. Massive primordial black holes as dark matter and their detection with gravitational waves. In *Journal of Physics: Conference Series*, volume 840, page 012032. IOP Publishing, 2017.
- [32] Nelson Pinto-Neto. Bouncing quantum cosmology. *Universe*, 7(4):110, 2021.
- [33] Robert Brandenberger and Patrick Peter. Bouncing cosmologies: Progress and problems. *Foundations of Physics*, 47(6):797–850, feb 2017.
- [34] S. D. P. Viteni, F. T. Falciano, and N. Pinto-Neto. Covariant bardeen perturbation formalism. 2013.
- [35] M. Gasperini and G. Veneziano. Inflation, deflation, and frame-independence in string cosmology. *Mod. Phys. Lett. A*, 8:3701–3713, 1993.
- [36] M. Gasperini and G. Veneziano. Dilaton production in string cosmology. *Phys. Rev. D*, 50:2519–2540, 8 1994.

- [37] David H Lyth. The primordial curvature perturbation in the ekpyrotic universe. *Physics Letters B*, 524(1-2):1–4, 2002.
- [38] Fabio Finelli and Robert Brandenberger. Generation of a scale-invariant spectrum of adiabatic fluctuations in cosmological models with a contracting phase. *Physical Review D*, 65(10):103522, 2002.
- [39] D. Wands. Duality invariance of cosmological perturbation spectra. *Phys. Rev. D*, 60(2):023507, 7 1999.
- [40] R. Brandenberger and F. Finelli. On the spectrum of fluctuations in an effective field theory of the ekpyrotic universe. *J. High Energy Phys.*, 11:56, 11 2001.
- [41] Patrick Peter and Nelson Pinto-Neto. Primordial perturbations in a nonsingular bouncing universe model. *Phys. Rev. D*, 66(6):063509, sep 2002.
- [42] J. Hwang and H. Noh. Non-singular big-bounces and evolution of linear fluctuations. *Phys. Rev. D*, 65:124010, 2002.
- [43] S. D. P. Vitenti and N. Pinto-Neto. Primordial power spectrum from a contracting pre-bounce phase. In Thibault Damour, Robert Jantzen, and Remo Ruffini, editors, *The Twelfth Marcel Grossmann Meeting: On Recent Developments in Theoretical and Experimental General Relativity, Astrophysics and Relativistic Field Theories: Proceedings of the MG12 Meeting on General Relativity*, pages 1424–1426. World Scientific Publishing Company, 2012.
- [44] SDP Vitenti, FT Falciano, and N Pinto-Neto. Quantum cosmological perturbations of generic fluids in quantum universes. *Physical Review D*, 87(10):103503, 2013.
- [45] Diana Battafield and Patrick Peter. A critical review of classical bouncing cosmologies. *Physics Reports*, 571:1–66, apr 2015.
- [46] Patrick Peter, Emanuel JC Pinho, and Nelson Pinto-Neto. Noninflationary model with scale invariant cosmological perturbations. *Physical Review D*, 75(2):023516, 2007.
- [47] Ivan Agullo, Javier Olmedo, and V Sreenath. Observational consequences of bianchi i spacetimes in loop quantum cosmology. *Physical Review D*, 102(4):043523, 2020.
- [48] Mairi Sakellariadou. Phenomenology of loop quantum cosmology. In *Journal of Physics: Conference Series*, volume 222, page 012027. IOP Publishing, 2010.
- [49] BJ Carr and AA Coley. Persistence of black holes through a cosmological bounce. *International Journal of Modern Physics D*, 20(14):2733–2738, 2011.
- [50] Maxence Corman, William E East, and Justin L Ripley. Evolution of black holes through a nonsingular cosmological bounce. *Journal of Cosmology and Astroparticle Physics*, 2022(09):063, 2022.
- [51] Jie-Wen Chen, Junyu Liu, Hao-Lan Xu, and Yi-Fu Cai. Tracing primordial black holes in nonsingular bouncing cosmology. *Physics Letters B*, 769:561–568, 2017.
- [52] Jie-Wen Chen, Mian Zhu, Sheng-Feng Yan, Qing-Qing Wang, and Yi-Fu Cai. Enhance primordial black hole abundance through the non-linear processes around bounce point. *Journal of Cosmology and Astroparticle Physics*, 2023(01):015, 2023.
- [53] Jerome Quintin and Robert H. Brandenberger. Black hole formation in a contracting universe. *Journal of Cosmology and Astroparticle Physics*, 2016(11):029–029, November 2016.

- [54] Sandro Dias Pinto Vitenti and Nelson Pinto-Neto. Large adiabatic scalar perturbations in a regular bouncing universe. *Physical Review D*, 85(2):023524, 2012.
- [55] Nelson Pinto-Neto. Quantum cosmology: how to interpret and obtain results. *Brazilian Journal of Physics*, 30:330–345, 2000.
- [56] Richard C. Tolman. *Relativity, Thermodynamics and Cosmology*. Dover, 1934.
- [57] Abbé Georges Lemaître. l’Univers en expansion. *Annales de la Société Scientifique de Bruxelles*, A 53:51, 1933.
- [58] Nelson Pinto Neto. *Hamiltonian formulation of General Relativity and applications*. Cadernos de Astrofísica, Cosmologia e Gravitação. PPGCosmo, 2020.
- [59] Jonathan J Halliwell. Introductory lectures on quantum cosmology. *Introductory lectures on quantum cosmology*, 1990.
- [60] N. Pinto-Neto and J. C. Fabris. Quantum cosmology from the de broglie-bohm perspective. 2013.
- [61] Bryce S DeWitt. Quantum theory of gravity. i. the canonical theory. *Physical Review*, 160(5):1113, 1967.
- [62] Claus Kiefer and Patrick Peter. Time in quantum cosmology. *Universe*, 8(1):36, 2022.
- [63] Przemysław Małkiewicz, Patrick Peter, and SDP Vitenti. Quantum empty bianchi i spacetime with internal time. *Physical Review D*, 101(4):046012, 2020.
- [64] Viatcheslav Mukhanov. *Physical foundations of cosmology*. Cambridge university press, 2005.
- [65] J. M. Bardeen. Gauge-invariant cosmological perturbations. *Phys. Rev. D*, 22:1882–1905, 10 1980.
- [66] Viatcheslav F Mukhanov, Hume A Feldman, and Robert Hans Brandenberger. Theory of cosmological perturbations. *Physics reports*, 215(5-6):203–333, 1992.
- [67] Viatcheslav F Mukhanov and GV Chibisov. Quantum fluctuations and a nonsingular universe. *ZhETF Pisma Redaktsiiu*, 33:549–553, 1981.
- [68] Stephen W Hawking. The development of irregularities in a single bubble inflationary universe. *Physics Letters B*, 115(4):295–297, 1982.
- [69] Robert M Wald. *Quantum field theory in curved spacetime and black hole thermodynamics*. University of Chicago press, 1994.
- [70] Nicholas David Birrell and Paul Charles William Davies. *Quantum fields in curved space*. 1984.
- [71] V. Mukhanov and S. Winitzki. *Introduction to Quantum Effects in Gravity*. Cambridge University Press, 2007.
- [72] Mariana Penna-Lima, Nelson Pinto-Neto, and Sandro DP Vitenti. New formalism to define vacuum states for scalar fields in curved space-times. *arXiv preprint arXiv:2207.08270*, 2022.
- [73] Sandro Dias Pinto Vitenti and M. Penna-Lima. NumCosmo: Numerical Cosmology. Astrophysics Source Code Library ascl:1408.013, aug 2014.
- [74] Carlton Baugh and P Murdin. Correlation function and power spectra in cosmology. *Encyclopedia of Astronomy and Astrophysics, (IOP, London, UK, 2006)*, 2006.

- [75] Planck Collaboration. Planck 2018 results. x. constraints on inflation. 2018.
- [76] Yi Wang and Wei Xue. Inflation and alternatives with blue tensor spectra. *Journal of Cosmology and Astroparticle Physics*, 2014(10):075–075, October 2014.
- [77] Y.-F. Cai and E. Wilson-Ewing. A  $\Lambda$ cdm bounce scenario. *J. Cosmol. Astropart. Phys.*, 3:006, March 2015.
- [78] Sachiko Kuroyanagi, Tomo Takahashi, and Shuichiro Yokoyama. Blue-tilted inflationary tensor spectrum and reheating in the light of nanograv results. *Journal of Cosmology and Astroparticle Physics*, 2021(01):071, 2021.
- [79] Yu-Mei Wu, Zu-Cheng Chen, and Qing-Guo Huang. Search for stochastic gravitational-wave background from massive gravity in the nanograv 12.5-year dataset. *Physical Review D*, 107(4):042003, 2023.
- [80] Ilia Musco. Threshold for primordial black holes: Dependence on the shape of the cosmological perturbations. *Physical Review D*, 100(12), dec 2019.
- [81] James M Bardeen, JR Bond, Nick Kaiser, and AS Szalay. The statistics of peaks of gaussian random fields. *Astrophysical Journal, Part 1 (ISSN 0004-637X)*, vol. 304, May 1, 1986, p. 15-61. *SERC-supported research.*, 304:15–61, 1986.
- [82] Jérôme Martin, Christophe Ringeval, Roberto Trotta, and Vincent Vennin. The Best Inflationary Models After Planck. *J. Cosmol. Astropart. Phys.*, 1403:039, 2014.
- [83] Wolfram Research, Inc. Mathematica, Version 14.0. Champaign, IL, 2024.
- [84] Dipanjan Dey, NT Layden, AA Coley, and Pankaj S Joshi. The equilibrium condition in gravitational collapse and its application to a cosmological scenario. *arXiv preprint arXiv:2303.16789*, 2023.
- [85] Bernard Carr, Kazunori Kohri, Yuuiti Sendouda, and Jun’ichi Yokoyama. Constraints on primordial black holes. *Reports on Progress in Physics*, 84(11):116902, 2021.
- [86] William H Press and Paul Schechter. Formation of galaxies and clusters of galaxies by self-similar gravitational condensation. *The Astrophysical Journal*, 187:425–438, 1974.
- [87] Yi-Fu Cai, Chengfeng Tang, Geyu Mo, Sheng-Feng Yan, Chao Chen, Xiao-Han Ma, Bo Wang, Wentao Luo, Damien Easson, and Antonino Marciano. Primordial black hole mass functions as a probe of cosmic origin. *arXiv preprint arXiv:2301.09403*, 2023.
- [88] Xiao-Ming Bi, Lu Chen, and Ke Wang. Primordial black hole mass function with mass gap. *Monthly Notices of the Royal Astronomical Society*, 527(2):3962–3967, 2024.
- [89] Bernard Carr, Florian Kühnel, and Marit Sandstad. Primordial black holes as dark matter. *Physical Review D*, 94(8), oct 2016.
- [90] Cristian Armendariz-Picon and Jayanth T Neelakanta. How cold is cold dark matter? *Journal of Cosmology and Astroparticle Physics*, 2014(03):049, 2014.
- [91] Sérgio MCV Gonçalves. Black hole formation from massive scalar field collapse in the einstein–de sitter universe. *Physical Review D*, 62(12):124006, 2000.
- [92] SDP Vitenti, FT Falciano, and N Pinto-Neto. Covariant bardeen perturbation formalism. *Physical Review D*, 89(10):103538, 2014.